DESIGN AND SYNTHESIS OF A NOVEL NACREOUS-ENHANCED COMPOSITE FOR THE IMPROVED FIXATION OF LUMBAR TOTAL DISC REPLACEMENT

A Thesis

by

JOHN MASON REEKS

Submitted to the Office of Graduate and Professional Studies of
Texas A&M University
in partial fulfillment of the requirements for the degree of

MASTER OF SCIENCE

Chair of Committee,	Hong Liang
Co-Chair of Committee,	Alex Fang
Committee Member,	Melissa Grunlan
Head of Department,	Ibrahim Karaman

May 2016

Major Subject: Materials Science and Engineering

ABSTRACT

Adults suffering from lower back pain often find that the cause of pain is degenerative disc disease. While non-surgical treatment is preferred, spinal fusion and total disc replacement remain surgical options for the patient. Total disc replacement is an emerging and improving treatment for degenerative discs. This research studies effects of microstructure of a novel composite on mechanical properties and investigates the potential application in total disc replacements. A systematic approach was taken to conduct this research. This approach includes the design of a three-component composite, fabrication of samples of the proposed composite, the characterization of the samples and their evaluation and ranking. Samples were ranked based on viability as an implant material. To validate the samples as possible implant materials, experiments were conducted to evaluate the tribological performance, corrosion resistance, scratch resistance, and bioactivity of the samples. Results showed that samples with 25wt% PP performed best with respect to tribological performance and scratch resistance while 33wt% samples had the best corrosion resistance. These results indicate that nacreous-enhanced composites show promise for improving the fixation of TDR and require further research and optimization.

DEDICATION

I would like to dedicate this thesis to my parents, F. John and Gretchen, and to my brother, Michael for their continued love and support.

ACKNOWLEDGEMENTS

Special thanks to Dr. Liang, my advisor, as well as my committee members: Dr. Melissa Grunlan and Dr. Alex Fang for supporting my education and research. Additionally, I thank all of the members of the surface science group for help and advice throughout.

TABLE OF CONTENTS

Page

LIST OF FIGURES

Page

LIST OF TABLES

Page

CHAPTER I

INTRODUCTION[*]

This chapter provides basic information to aid in the audience's understanding of the goals of this thesis. It begins by introducing the lumbar spine and its roles followed by a description of the intervertebral disc and Total Disc Replacement. The content of this chapter has been published: Reeks, J., & Liang, H. (2015). Materials and Their Failure Mechanisms in Total Disc Replacement. *Lubricants*, *3*(2), 346-364.

1.1 The Lumbar Spine

1.1.1 Lower Back Pain and the Intervertebral Disc

Lower back pain (LBP) is among the most common ailments for adults in the United States. According to a national survey performed by the CDC, 28.8% of adults have complaints of lower back pain [1]. Many cases of LBP are caused by intervertebral disc (IVD) injury or degenerative disc disease (DDD) or other disc injury. The IVD relies on natural flexibility of its materials as well as its pseudo-pneumatic structure to transmit loads down the spine even in awkward loading positions [2]. In addition to transmitting loads and maintaining structure, the natural IVD behaves as a "hydrodynamic ball bearing" [2] allowing for smooth rotational motion. Natural IVD permits angular movement in the 3 planes of motion (sagittal, lateral, and transverse)

[*] Adapted from: Reeks, J., & Liang, H. (2015). Materials and Their Failure Mechanisms in Total Disc Replacement. Lubricants, 3(2), 346-364. MDPI is an open access journal in which the author retains copyright. (MDPI.com)

giving it 6 degrees of freedom (DOF) [2-4]. This characteristic of the IVD is unlike any other joint. The balance of motion and motion resistance allow the body to maneuver in a complex manner while minimizing the stress induced by other parts of the body. Unfortunately, the requirement that it simultaneously undergo torsion, shear stress, localized compressive stress, and localized tensile stress both causes DDD and creates problems for treatment thereof.

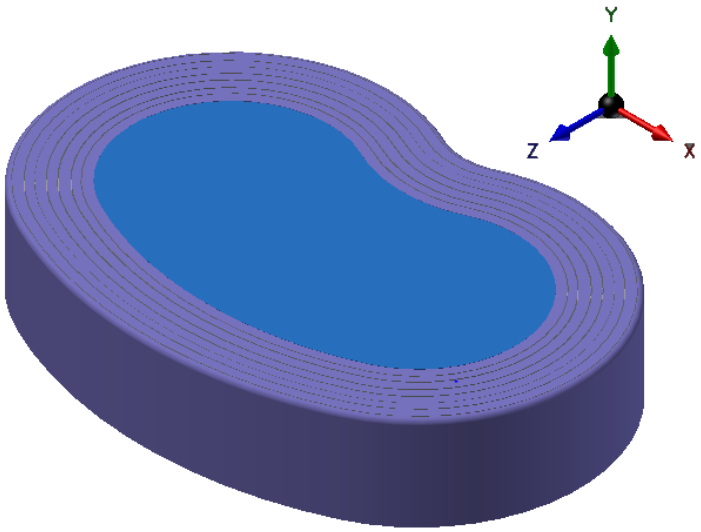

Figure 1 Drawing of the structure of an intervertebral disk.

A simple model of the IVD is shown in Figure 1. It is composed of a nucleus pulposus (inner structure) and the annulus fibrosus (outer structure). The nucleus can absorb some impact between adjacent vertebral bodies, thus protecting the rigid vertebral bodies from each other. The pulposus also acts to preserve the disc itself by helping withstand compression [4]. Surrounding the nucleus is the lamellar [2, 4] annulus fibrosus. The annulus is composed of layers of oriented collagen fibers [4, 5]. The collagen fibers in the annulus are arranged such that the fibers of every other layer have the same orientation. The adjacent layers, however have the opposite orientation [4, 6-8]. These fibers are generally positioned at a 65^{o} angle from the y axis in the figure above [4].

One treatment for DDD is spinal fusion. This treatment method alleviates pain, but limits range of motion (ROM) and mobility for the patient. Total disc replacement (TDR) is another treatment method for DDD that aims to preserve motion and limit complications related to spinal fusion such as adjacent level wear and disc degeneration [8-12]. This motion preservation is critical to preventing wear and injury in the area surrounding the treated disc. By inhibiting motion, fusion creates stress concentrations at adjacent level facets and discs [9, 12-14]. TDR is performed in an effort to solve these issues and help maintain normal range or motion for patients [11].

Although the preservation of motion through TDR alleviates some problems associated with spinal fusion, TDR introduces different types of problems and failures. TDR creates issues and problems not seen in other implants and vary based on the

design of the TDR implant. The primary issues and problems associated with TDR are hyper-mobility, hypo-mobility, material wear, and wear debris particles.

1.2 Lumbar Total Disc Replacements

To be effective, TDR implants must satisfy three requirements. The implant must have a solid, nondestructive interface with the adjacent vertebral bodies; provide mobility; and resist wear. This thesis will focus on problems associated with the interface of the implant with adjacent vertebral bodies. More strength and durability is required of lumbar implants than implants in the cervical area due to the extra loads it must bear. The lumbar spine supports more weight and encounters movements of greater magnitude than the cervical spine [15].

Device	Classification	Biomaterials	Bearing Design	References	Manufacturer
CHARITE	MoP	CoCr-UHMWPE	Mobile	[10, 16-19]	DePuy Spine
Prodisc-L	MoP	CoCr-UHMWPE	Fixed	[16, 20]	DePuy Synthes
Activ-L	MoP	CoCr-UHMWPE	Mobile	[21]	Aesculap
Mobidisc	MoP	CoCr-UHMWPE	Mobile	[10, 22]	LDR Medical
Baguera	MoP	DLC coated Ti-UHMWPE	Fixed	[16]	Spineart
NuBac	PoP	PEEK-PEEK	Fixed	[23]	Pioneer
Maverick	MoM	CoCr-CoCr	Fixed	[16]	Medtronic
Kineflex	MoM	CoCr-CoCr	Mobile	[10, 16]	SpinalMotion
Flexicore	MoM	CoCr-CoCr	Constrained	[10]	Stryker
XL-TDR	MoM	CoCr-CoCr	Fixed	[10, 24]	NuVasive
CAdisc-L	One piece (1P)	PU-PC graduated modulus	1P	[10, 16, 25]	Rainier Technology
Freedom	1P	Ti plates; silicone PU-PC core	1P	[10, 16]	Axiomed
eDisc	1P	Ti plates; elastomer core	1P	[10, 16]	Theken
Physio-L	1P	Ti plates; elastomer core	1P	[10, 16, 26, 27]	NexGen Spine
M6-L	1P	Ti plates; PU-PC core with UHMWPE encapsulation	1P	[16]	Spinal Kinetics
LP-ESP (elastic spine pad)	1P	Ti endplates; PUPC coated silicone gel	1P	[3]	FH Orthopedics

Table 1 Summary of current TDR classification, materials, bearing type and regulatory status

1.2.1 Types of Lumbar TDR

Except for those classified as 1P bearings, the designs shown in Table 1 involve a ball and socket design. A fixed bearing involves no moving parts except the sliding of the socket over the ball, but mobile and constrained bearings permit motion of the ball component. All of the above designs interface with the adjacent vertebrae with Titanium endplates.

1.2.1.1 Ball and Socket

When designing the ball and socket TDR, a major source of inspiration is the total hip replacement. Hip replacements use a ball and socket design and experience higher stress and load concentrations than what is needed for TDR. Material selection therefore is often inspired by materials used in hip replacement prostheses. The sliding surfaces for the ball and socket bearings are composed of CoCr-CoCr for MoM designs and CoCr-UHMWPE for MoP designs. CoCr alloys are used because they have been found to produce less wear debris in knee and hip replacements [10]. Figure 2 is a drawing of the ball and socket mechanism in these devices to roughly illustrate how they work.

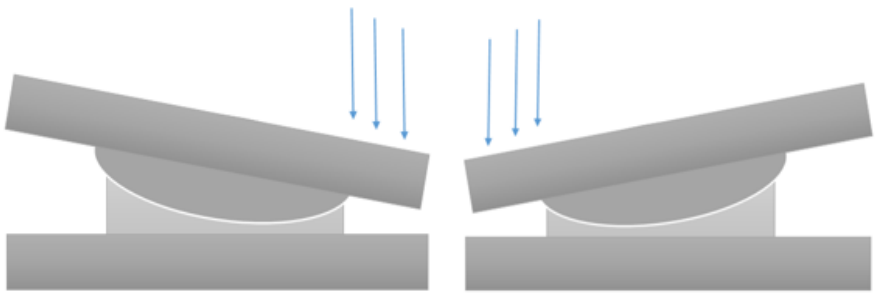

Figure 2 Illustration of working mechanisms of ball-socket devices.

1.2.1.2 One Piece

The one piece bearing design is a recent development for TDR. The purpose of this design is to more closely mimic the natural disc behavior through the implant. One piece designs reduce the number of surfaces on which wear can occur and they reduce hypermobility of the joint. Additionally, since these implants are made of a softer elastomer, they also imitate the cushioning provided by the natural intervertebral disc.

The goal of TDR is to be an effective treatment for lumbar DDD. More specifically, studies show that the elastomeric 1P bearing TDR are the future of DDD treatment [51, 52]. These 1P bearings provide a solution to common problems seen with ball and socket TDR implants [21]. A hurdle for these designs is finding suitable core materials for biocompatibility and adhesion to the vertebral bodies [26]. This problem seems to have been solved by the use of the PUPC cores in the one piece (1P) bearing implant design, but more research is still to be done for these designs [16]. The 1P design limits particle driven osteolysis, but mechanically driven osteolysis and fixation issues due to mechanical incompatibility would continue to be problematic.

1.2.2 Bone-Implant Interface

A problem that distinguishes TDR from joint replacements in other parts of the body lies in the complex duty of the intervertebral disc. It is not merely a joint connecting two moving parts. The intervertebral disc, especially in the lumbar region, serves to resist motion and reduce stress concentrations in the adjacent level vertebrae and tissue [4,9].

The Spine Institute at The Ohio State University (OSU) used a unique hybrid biomechanical model to analyze lumbar function after implantation of Prodisc-L TDR (one of the more popular ball-and-socket designs) under different external loading conditions. This model was made after an individual male and uses a flexible multi-body dynamic analysis system [9]. The model looked at TDR at all lumbar levels, and examined vertebral body loading, ROM, and ligament and facet joint forces. These measurements were taken when the subject was not exerting at all and when he was asked to lift 9.5 and 19 kg separately. The figures below are drawn based on the OSU study. In the figures, the abbreviations SUP and INF represent the interface at the superior and inferior levels of the implant respectively. Figure 3 [9] shows mean values of data from a virtual model simulation of vertebral loadings from the OSU study at different implantation levels. The original data can be found in reference [9]. Before reviewing these data some terminology should be reviewed. Numbers such as L5 and S1 describe specific vertebrae. L5 is the fifth and most inferior lumbar (L) vertebrae. S1 is representative of the sacrum which is inferior to the lumbar spine and is immobile.

Figure 3, Figure 4, and Figure 5 below show approximate mean value data for different simulated loadings based on disc type and implantation level. The information is organized such that data for a given implantation level are reported in the same color. The study found that the substantial differences in performance between TDR and the natural disc were closer to L5/S1 level. Therefore, the information below focuses on that region. After examining Figure 3 it can be noted that in general at lower lumbar levels (L4/L5 to L5/S1) that compressive loads increase after implantation. These loading

changes are primarily due to high stiffness of the implant and discontinuity at the bone-implant interface. Similar trends of excess loadings due to TDR can be noted for vertebral body shear loadings as well. In the case of AP shear loading, seen in Figure 5 the direction and magnitude of the shear are dependent upon the shape of the spine. Since the resistance to motion is less with TDR, less shear loading is exhibited with TDR than an intact disc in regions of spinal curvature. This, however would indicate higher loading of the nearby ligaments.

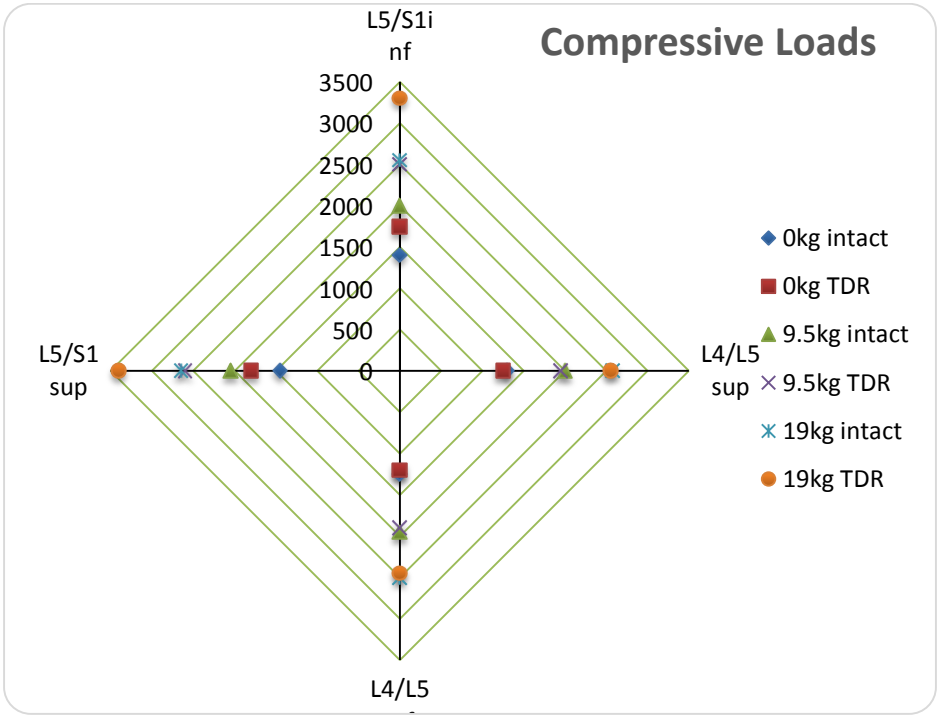

Figure 3 Comparison of simulated compressive vertebral loads before and after TDR implantation, based on exterior loading and implantation level [9].

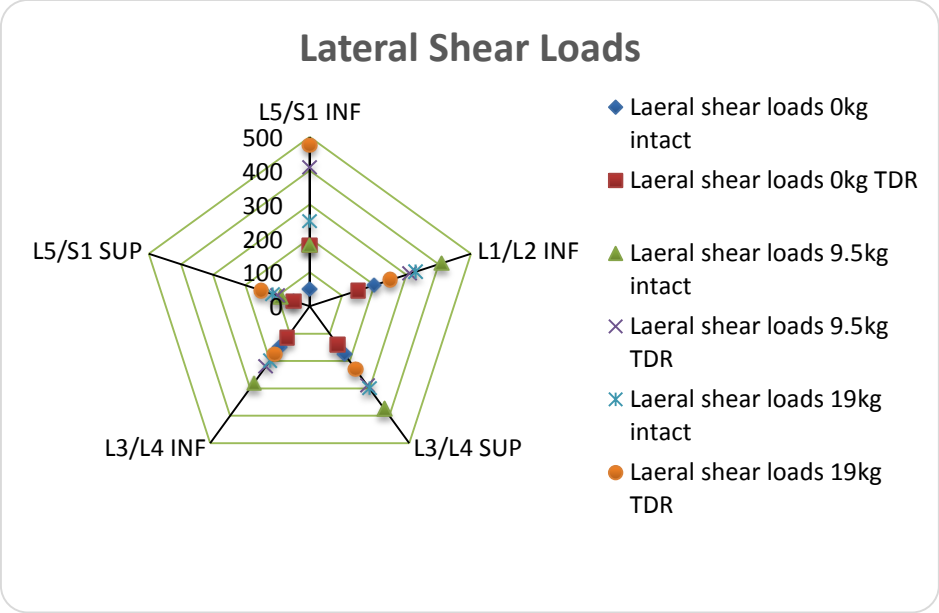

Figure 4 Comparison of simulated anterior-posterior shear loading at vertebral body interface before and after TDR implantation based exterior loading and implantation level [9].

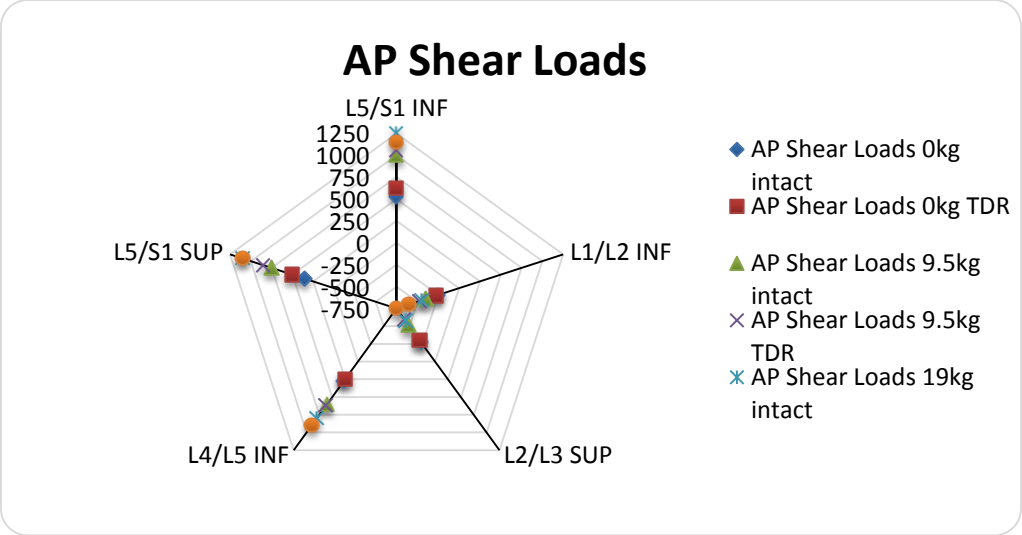

Figure 5 Comparison of simulated lateral shear loading at vertebral body interface before and after TDR implantation based on exterior loading and implantation level [9].

1.2.3 Interface Failure

1.2.3.1 Osteolysis

Osteolysis is a mode of degradation which involves the destruction of bone [28]. In the case of orthopedic implants and arthroplasty, osteolysis occurs at the interface between bone and implant.

Osteolysis is a prominent mode of failure for total joint replacements including TDR [29]. Some studies suggest osteolysis isn't as prevalent in TDR due to the fact that there is a smaller range of motion in TDR than in hip and knee replacements which would indicate smaller wear tracks and fewer debris particles. These and other sources, however, do indicate that these wear particles remain a concern in spinal implants

because they indirectly induce osteoclastogenesis which can lead to bone resorption and inflammation [16, 30-32].

1.2.3.1.1 Motion Driven Osteolysis

Motion driven osteolysis in TDR implants is a result of micro-motion of the implant against the adjacent body [33]. Figures 3, 4, and 5 above compare vertebral body loadings of a natural disc to the Prodisc articulating TDR. While there is not a substantial difference in shear loadings, normal loadings would increase friction and wear between the device and vertebrae. It is easy to picture how motion would cause bone degeneration: just like the periodic maneuvering of a shovel in soft clay will loosen and remove some clay. The osteolytic response to debris particles, however, is not so straight forward.

1.2.3.1.2 Particle Driven Osteolysis

In TDR implants the biological response to wear debris is based on number of particles, particle size, particle shape, and chemical composition of the debris [34]. This indicates that biological responses in TDR are design and material dependent. Material independent responses include inflammation and osteolysis. Osteolysis is often a result of the inflammatory response.

Bone growth and maintenance are the results of equilibrium responses of bone growth and resorption which are driven by osteoblasts and osteoclasts, respectively. Debris particles disrupt bone homeostasis [34] through an inflammatory response which

in turn stimulates the maturation of osteoclasts increasing bone resorption [33, 34]. The combination of these wear processes leads to increased wear rates over time as resorption loosens the device thus creating more space for osteolysis-causing motion and debris [35].

1.3 Nature-inspired Materials: Pearl Powder and Nacre

1.3.1 Structure and Mechanical Properties

Seashells have inspired many biomimetic designs. The microstructure found in seashells, which is particularly interesting, is nacre. Nacre is composed of aragonite calcium carbonate platelets interconnected by a natural protein matrix. This unique structure turns what would normally be a relatively weak but hard ceramic into a tough, lightweight, protective structure. Surface Science Group at Texas A&M has published multiple papers involving the use of natural nacre to improve wear and corrosion resistance of engineering materials [36, 37]. This is a sacrificial protection method as Calcium is more active than metal matrix materials like aluminum and will be attacked preferentially in an ionic environment [36].

In addition to its use in wear and corrosion resistance, nacre also shows promise for use in orthopedics. It has a comparable Young's Modulus 30-40 GPa as opposed to 20 GPa for bone [38].

1.3.2 Osteoconductive Properties

Nature made materials often have properties and structures that are far more intricate than those produced synthetically. Pearls and seashells are no exception. The

nacre produced by these animals not only contains the $CaCO_3$ that promotes bone growth but the proteins that bind the aragonite platelets behave as signal proteins [39-43]. These signal proteins emit signals that tell the body to initiate repair and signal growth. This is why pearl powder is commonly used in health and beauty products to heal scars and repair skin [39, 44]. With regard to bone, the pearl nacre promotes the densification of bone as well [39].

Pearl powder has been reported as a natural and biocompatible material to promote bone growth [38, 42]. Studies have shown that when nacre is introduced to bone or bone defects there is a direct "welding" of bone to nacre [38, 45]. These studies indicate that pearl nacre exhibits extraordinary osteoconductivity and potential to speed bone building and recovery [39, 46].

CHAPTER II

MOTIVATION AND OBJECTIVES

2.1 Motivation

As discussed in Chapter I above, Total Disc Replacement and other orthopedic implants have a tendency to fail at the interface between bone and implant. This failure can be caused by osteolysis and other biological or immune reactions to the implant or debris from the implant. One way to combat these failure modes is to enhance the implant where it interfaces with the bone. Currently this is done primarily with rough texturing to allow trabecular tissue to grow into the texture and form a grip. Even if the texture has an osteoconductive coating, current designs would not combat long-term osteolysis. Nacre is an osteoconductive material with strong mechanical properties. A composite material utilizing its properties could allow bone to grow into the bulk of the material and not only enhance the grip on the device but could prevent reactive debris from infiltrating the interface.

2.2 Objectives

There are three primary objectives in this research. The ultimate goal of this research is to design and show feasibility of a novel composite suitable for applications in bone fixation of the TDR. The objectives are as follows:

1. Develop a new bio-inspired composite
2. Obtain understanding of properties and performance
3. Establish the validity of the material

In order to achieve our goal, this research uses experimental approaches to design, synthesize, evaluate, and characterize the sample materials made. This is discussed below in Chapter 3.

CHAPTER III

SAMPLE PREPARATION

This chapter outlines the rationale and design of the composite. The fabrication methodology is then outlined. Characterization techniques are discussed at the end of the chapter.

3.1 Composite Design Requirements

The proposed composite needs to satisfy the following criteria. It must be:

1. Resistant to corrosion;
2. Wear resistant in corrosive environment;
3. Be Bioactive (promote bone ingrowth); and
4. Be less stiff than current interfacial materials

In order to produce a viable composite, the composite materials must contribute to at least one of the aforementioned criteria.

3.2 Materials

3.2.1 Pearl Powder

Due to the regenerative and healing properties of Pearl Powder, it is readily available at many beauty stores (Amazon is the source in this case). Pearl powder is selected as a bioactive material as well as an aid to corrosion resistance. Aragonite melts at 825^{o}C and has a density of 2.9 g/cm^{3}. $CaCO_3$ also decomposes into CaO and CO_2 at 840^{o}C. After microscopic examination to ensure the package contained only pearl

powder two batches of pearl powder were separated. Batch one was simply the pearl powder as it was delivered. Batch two was filtered through a sieve with a 53 micron mesh.

3.2.2 Titanium Powder

Since it is already a predominantly used biomaterial for this application, commercially pure titanium was used as a strengthening material for the composite. Both CP Ti and Ti6Al4V are commonly used for bone implant interface due to superior mechanical properties and corrosion resistance. Titanium is used in this composite for the same reasons that it is used in other orthopedic implants: it is wear and corrosion resistant. Titanium melts at 1660^{o}C and has a density of 4.5 g/cm^{3}. This high melting point, and therefore sintering temperature, is an issue which will be discussed in the next section.

3.2.3 Aluminum Powder

Titanium cannot be the sole matrix for this composite for two reasons: it must be processed at a higher temperature than the decomposition point of $CaCO_3$ and it is much more stiff than bone which causes a discontinuity at the bone interface. Aluminum is introduced as a bonding matrix to lower the processing temperature and the stiffness of the compositeAluminum is not generally used for this type of application, but it is softer than Ti and through the use of nacre corrosion resistance is greatly improved [36, 37]. Figure 6 shows how nacreous $CaCO_3$ protects Al from corrosion. Aluminum melts at 660^{o}C and has a density of 2.7 g/cm^{3}.

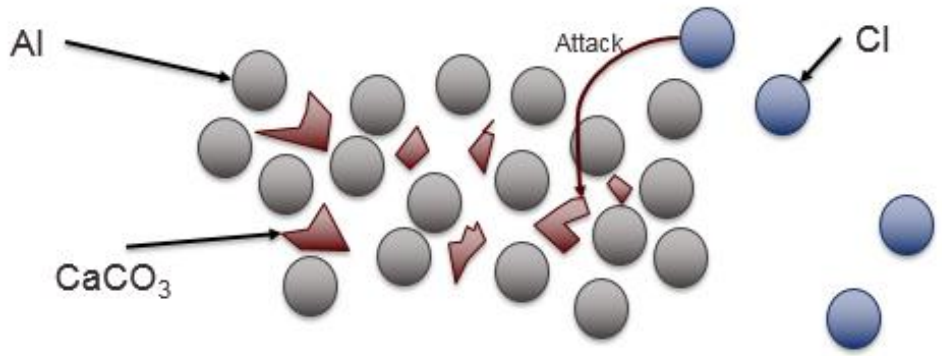

Figure 6 Nacre protects aluminum

3.3 Fabrication Process

Figure 7 below is a flowchart representing the fabrication process for the composites.

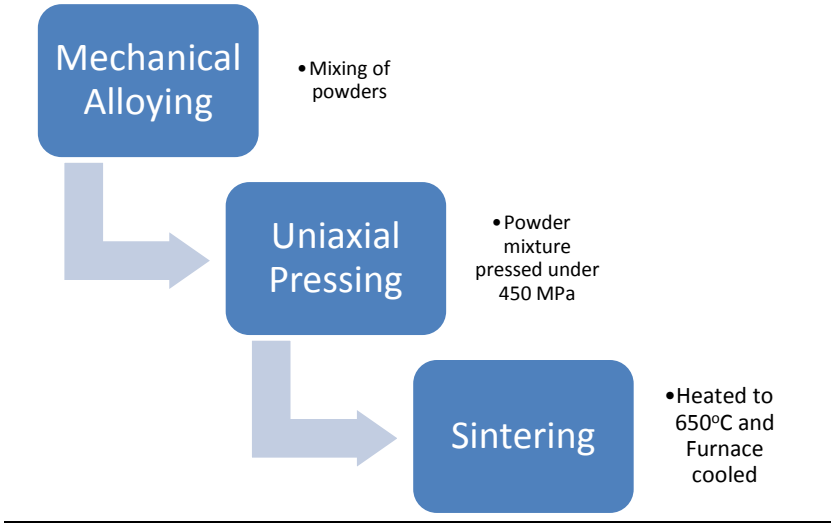

Figure 7 Fabrication flowchart

3.3.1 Mixing

Powder mixtures were made of several different compositions prior to compaction. Each powder combination was mixed in a rotating mixer for 8 hours to ensure homogeneity.

This process became largely trial and error. Initially the mixture was composed of only pearl powder and titanium. These samples, however, were not strong. This is where the idea for adding aluminum originated. Ti-pearl powder composites did not bind well. Aluminum was added as a possible binding agent. Initially low concentrations of aluminum were tried, but because pearl powder has such a low density

the lower weight percentages of pearl powder occupy a substantial volume within the composite. This resulted in a relatively weak composite. The strongest composites of these of these materials contained a very high percentage of aluminum by volume, which would be an item for concern if not for its protection by the surrounding pearl powder. Since Titanium is the greatest obstacle to binding in this material, the weight ratio of Al to Ti was maintained constant in samples 1 through 6. The Al to Ti ratio in these samples was chosen experimentally through trial and error to find the strongest binding combination. This means the concentration of each metal changes sample to sample. The metal weight percentages of the different samples are shown below in Table 2.

Material	**Composition for each specimen (wt%)**						
	1	2	3	4	5	6	7
Aluminum	52.5	56.25	67.5	52.5	56.25	67.5	33.33
Titanium	17.5	18.75	22.5	17.5	18.75	22.5	33.33
PP unfiltered)	30	25	10				33.33
PP (filtered)				30	25	10	

Table 2 Sample compositions

3.3.2 Pressing

Compression is a common method for making green compacts (compacts prior to heat treatment). In this stage of manufacturing a composite, particle size and shape becomes important. Compression is used to press powders together to increase the overall density and to minimize porosity. This ensures that there is maximum interaction between particles during sintering. In this particular situation particle size and shape differences had a substantial effect on the properties of the green and sintered compact. This will be addressed below.

Powders were compacted uniaxially in a cylindrical die cavity having a diameter of 14 mm. Tool steel punches were used to press the powder. Compaction pressure for these samples was 450 MPa. This pressure was held for 5 minutes to ensure densification. The resulting compacts had a diameter of 14 mm and a height of approximately 5 mm. A schematic of the pressing is displayed below in Figure 8. To improve the uniformity, density, and mechanical properties the green compact must be sintered [47].

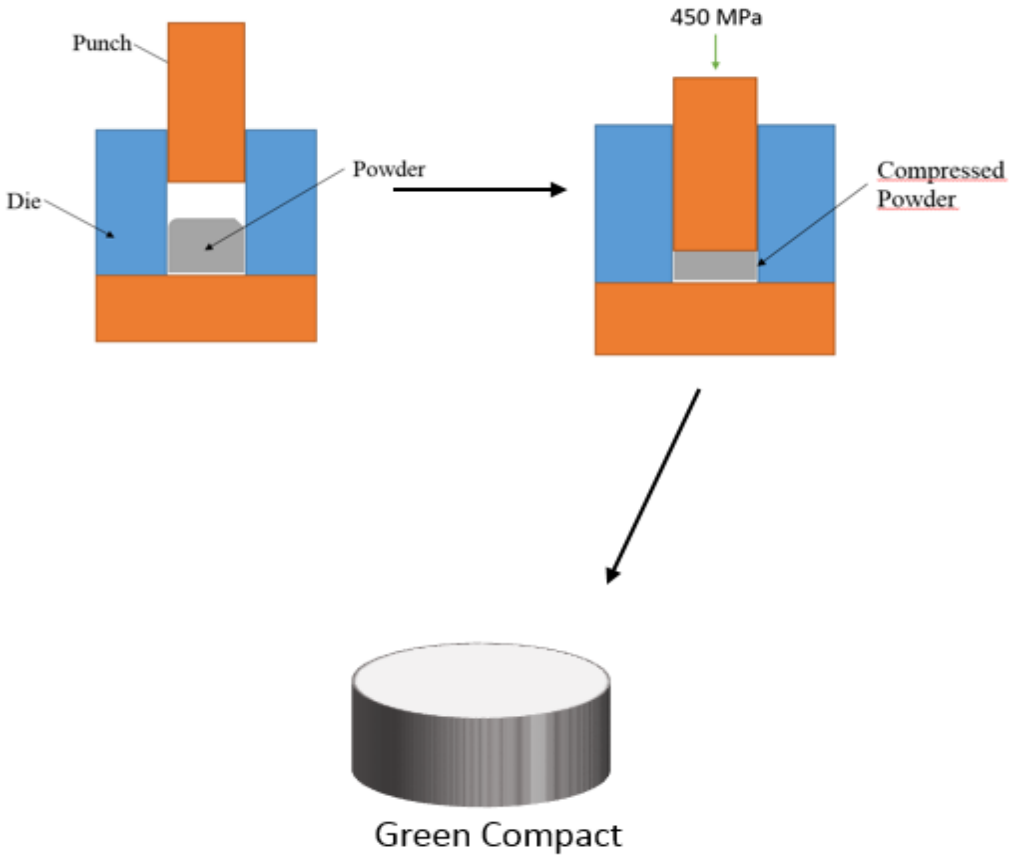

Figure 8 Powder pressing

3.3.3 Sintering

A Thermo Electron Corp furnace was used to sinter the compacts. In common practice sintering temperature is approximately 2/3 of the melting point of the materials. As mentioned above this would mean the $CaCO_3$ would decompose thermally before the titanium could be effectively treated. Having Aluminum introduced as a binder material can significantly lower the sintering temperature for these samples and allow for some

alloying of the metals to occur. The compacts were heated to 650^{o}C for 24 hours and furnace cooled.

Pure Al was selected as a bonding element that has relatively low Young's Modulus (about 70 GPa). Ti-Al alloys are stiffer than Al (Modulus 120 to 180 GPa [48]) and would increase the modulus mismatch between bone and implant. The phase diagram below indicates that there would be no phase transitions occurring at the sintering temperature (650^{o}C) allowed by $CaCO_3$. After examining Al-Ti phase diagram it is evident from this that no phase transition occurs at 650^{o}C for the selected concentrations of Ti and Al [49].

3.4 Characterization Methods

This chapter outlines the characterization methods used to evaluate and validate the proposed composite.

3.4.1 Wear Testing

3.4.1.1 Pin-On-Disc Tribometry

A pin on disc tribometer utilizes a spherical pin under an applied load to measure frictional and wear properties of a sample reciprocating or rotating beneath it. For this application the reciprocating mode of the tribometer was used. This is because the motion of the implant-bone interface is a reciprocating motion.

3.4.1.2 Wear Test Procedure

Prior to wear tests, samples were polished using 180, 400, and 800 grit SiC grinding paper. A CSM instruments pin-on-disc tribometer was used to carry out these wear tests. Figure 9 is a schematic illustrating how pin-on-disc tribometer works. The sample lies on a reciprocating stage beneath the bearing steel pin.

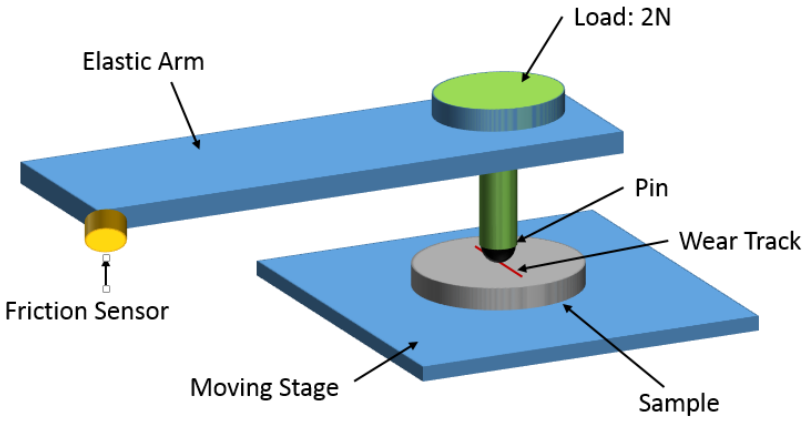

Figure 9 Pin-on-disc tribometer

Samples underwent the wear tests under a 2N normal load while immersed in a 2.73 Molar solution of NaCl. The test was run for a total sliding distance of 250 m with a sliding speed of 2cm/s. Using the rule of mixtures to determine the elastic properties of the composite, Hertzian contact can be estimated to be on the order of 100 MPa. This is orders of magnitude well above the stresses on the intervertebral disc. This was to assess the general wear and corrosion behavior since implants must operate in a corrosive environment.

Of the samples tested, the best performing sample, 25wt% PP,underwent a similar test using a piece of pork bone as a pin rather than the steel ball. Prior to use in

experimentation, the bone was cleaned and placed in boiling water for an hour then washed in an ethanol bath for sanitation. For these samples, loading conditions were chosen based on the stress experienced by lumbar intervertebral discs while standing: 1.1 MPa [50]. To replicate this loading, the bone was shaped such that the contact area with the sample was 1 mm^2. Adding a 2N load to this rather than 1N means the pressure experienced is 2MPa. This is done to anticipate excess loading of the device perhaps during activity or if the patient is wearing a backpack.

3.4.2 Porosity Measurement

Porosity in this case is measured using the water evaporation method. Measurement of the mass of the samples was taken both dry and saturated in deionized (DI) water. The difference in mass divided by the density of water yields pore volume which can be divided into total volume to determine porosity of the material. This will yield a qualitative understanding of porosity's contribution to other characteristics such as wear and corrosion.

3.4.3 Corrosion Resistance

Corrosion resistance is an important factor for proving the viability of any implant. This is to ensure reactive particles do not find their way into the patient's system. Establishing improvements in corrosion resistance through PP enhancement is important in establishing the proposed composite design.

3.4.3.1 Potentiodynamic Scan

When examining the corrosive properties of a material, its electrochemical response to an electrolyte solution can be observed. Since corrosion in an electrolyte

solution is a product of redox reaction, Faraday's law can be employed to quantify corrosive properties of a material. Faraday's law states that the amount of material consumed or the number of redox reactions occurring is proportional to the current passing through the electrolyte solution.

This means a lot of information can be determined by placing different potentials across the electrolyte solution and sample. When this is done a curve is produced which, in the case of normal metals, fits what is known as a Tafel curve as shown in Figure 10 below. On this curve the vertical axis represents the potential across the solution while the horizontal axis represents the current density on a $\log_{10}$ scale.

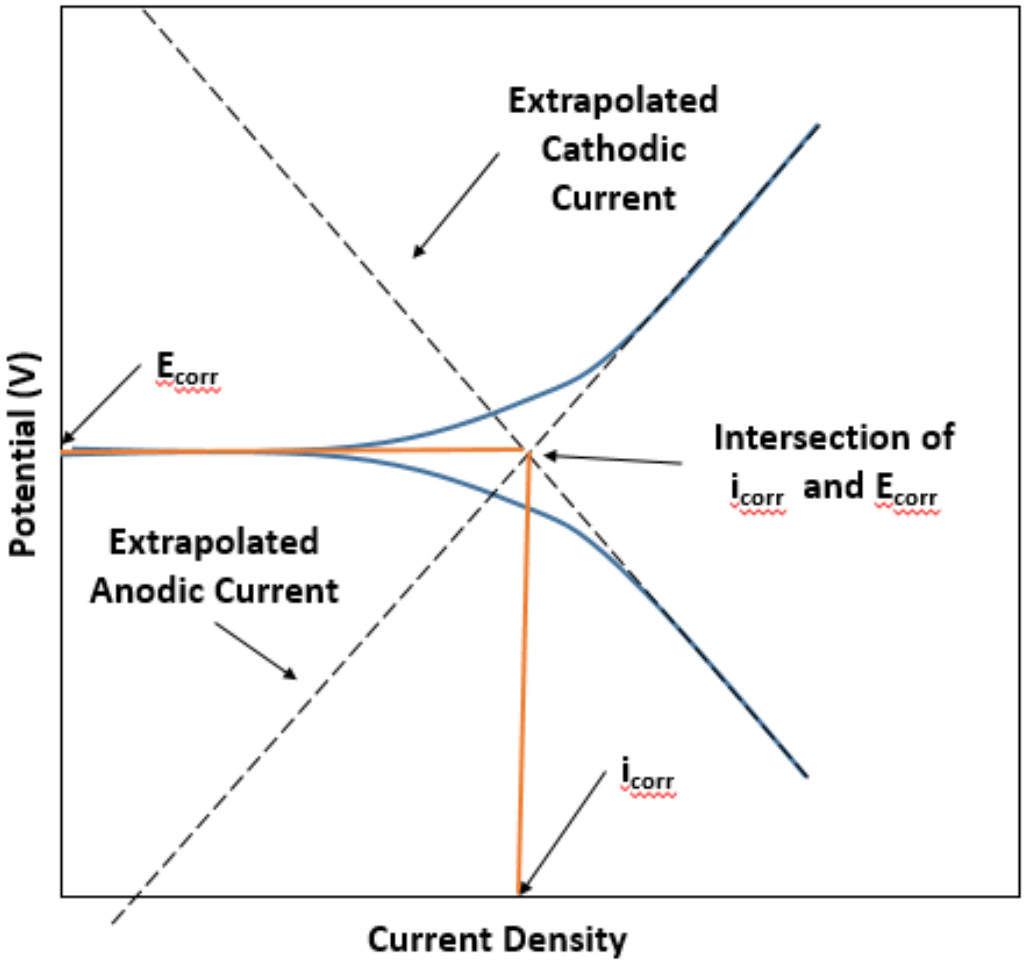

Figure 10 Tafel curve [36]

If the anodic and cathodic current curves are extrapolated (black dotted lines) they intersect with each other at the corrosion potential (E_{corr}). This point also yields the corrosion current (i_{corr}). Using this data corrosion rate can be calculated. The corrosion rate of a material is reported using the unit Mpy (mils per year). A mil is 1/1000 of an inch so this unit is a rate of consumption of the material being studied.

3.4.3.2 Corrosion Evaluation

The potentiodynamic polarization scan is executed using a Gamry instrument REF 600 as shown below in Figure 11. In the figure below the sample being tested is the working piece. The applied voltage for this measurement ranged from -2.0V to 2.0V in an electrolyte solution of 2.73 M NaCl.

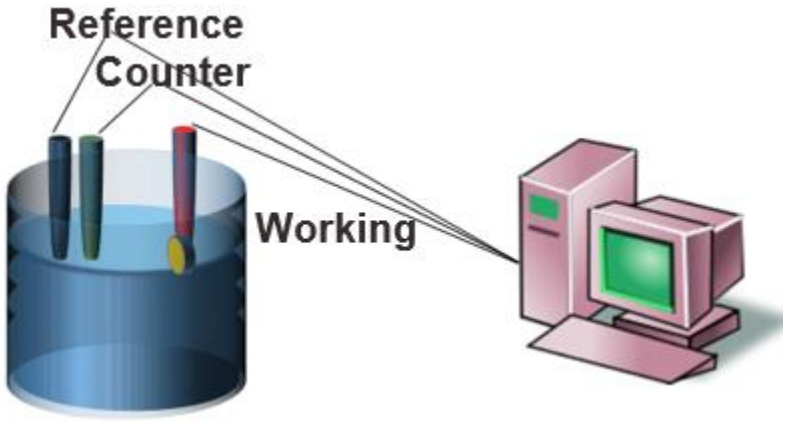

Figure 11 Schematic of corrosion test

3.4.4 *In vitro* Testing Using Simulated Body Fluid

3.4.4.1 Simulated Body Fluid

Since this material has application in orthopedics specifically for bone fixation it is important to understand how it would behave in the body. While it is not a fool proof test of bioactive materials, most materials bond to living bone through the formation of hydroxyapatite on the surface due to immersion in Simulated Body Fluid [51]. *In vitro* examination of bioactive surfaces and materials is done by immersing the material in Simulated Body Fluid (SBF) for several days. SBF is a solution which has the ion

concentration and pH similar to that of blood plasma and will induce apatite formation on the surface of bioactive materials [51].

3.4.4.2 Preparation of Simulated Body Fluid

SBF (1.0x) was prepared in the lab by dissolving the ingredients listed below in DI water following the procedure outlined by Kokubo [16, 51].

Order	Reagent	Amount
1	NaCl	8.035 g
2	NaHCO3	.355 g
3	KCL	.225 g
4	K2HPO4*3H2O	.231 g
5	MgCl2*6H2O	.311 g
6	1.0 M HCl	39 mL
7	CaCl2	.292 g
8	Na2SO4	.072 g
9	Tris	6.118 g
10	1.0 M HCl	0-5 mL

Table 3 Reagents and amounts for SBF preparation

3.4.4.3 Test Procedure

Selected samples were immersed in the SBF for 7 days and 14 days. After 7 days some samples were taken out and underwent XRD analysis. After 14 days in solution the rest of the samples were removed and examined using XRD, SEM, and optical microscopy.

3.4.5 Scratch Test

A scratch test was performed using the same tribometer used in wear testing. In this test, however, the tribometer was outfitted with a drill bit having an apex angle of 130^o under a 1 N Load. After this test is performed the track width and depth can be examined to calculate the fracture toughness of a material [52]. This can be used in comparison to bone to examine whether the material will withstand fracture better than human trabecular bone with which it will interface.

$$\frac{F_T}{K_c w\sqrt{d}} = \sqrt{2}\left(1 + 2\frac{d}{w}\right)^{1/2}.$$

Equation 1 Fracture toughness calculation [52]

Fracture toughness can be calculated using the above equation. In this equation K_c is fracture toughness, or fracture parameter, F_T is the tangential force required to produce the scratch, w is the width of the scratch, and d is the scratch depth.

CHAPTER IV

SAMPLE RANKING

This chapter discusses initial evaluation of the samples in order to select the best composition for the proposed composite. There are specific factors to be used as indicators of viability. The primary characteristics to consider are: wear resistance, corrosion resistance, bioactivity, porosity, and scratch resistance.

Characteristic	**Basis for Evaluation**
Wear Resistance	Limited wear in pin-on-disc, limited wear of bone
Corrosion Resistance	Increased nobility from metal matrix
Bioactivity	Precipitation of bone-like structure from Simulated Body Fluid
Porosity	Porosity an surface roughness to increase surface area without decreasing wear and corrosion resistance
Scratch Resistance	Exhibits adequate fracture toughness

Table 4 Characteristic evaluation

Almost immediately after processing, all of the samples made using the filtered pearl powders could be disqualified as possible candidates for this application. These samples were extremely brittle and porous. These particles were so much smaller than

the metal powders, causing a large variation in particle size throughout the compact. A large particle size distribution in this case leads to weaknesses in microstructure and increased porosity [53]. The resulting compacts both green and sintered were, therefore, too porous. This caused the samples to virtually disintegrate during polishing. While some degree of porosity is advantageous for bone ingrowth and bioactivity, too much porosity creates stress concentrations within the microstructure of the material ultimately making it weak. All of the samples made using the filtered pearl powder exhibited increased porosity and weakness. Samples, seemed to disintegrate during polishing.

4.1 Ranking Based on Wear Resistance

The first characterization method used in evaluating the samples was pin on disc tribometry. The experiments were conducted using the parameters are listed in Table 5.

Sample	Friction	Wear	Comments	Decisions
All Samples with filtered PP	N/A	N/A	Excessive wear under tribometry as well as polishing	Eliminate
10wt% PP	Did not stabilize	Excessive	Could not complete test due to excess wear	Eliminate
25wt%	Stabilizes	Limited Wear	Exhibits good wear resistance	Good
30wt%	Stabilizes	Limited Wear	Exhibits good wear resistance	Good
33wt%	Did not Stabilize	High Wear Rate	Does not exhibit good wear resistance	Bad

Table 5 Sample evaluation due to wear resistance

This evaluates how a material performs under long term loading and friction conditions. In the tribology tests using the steel pin, only samples containing 25 wt% PP, 30 wt% PP, and 33 wt% PP showed any resistance to wear. The other, more porous samples showed continuous wear even after the depth of the wear track exceeded the radius of the steel pin. This indicates that the more porous samples will wear in even

light loading. As a result, only the 25 wt% PP, 30 wt% PP, and 33 wt% PP samples were studied in the other tests.

Figure 12 is the wear scar produced on one of the porous specimen with the filtered PP. The excessive damage to this sample occurred very early in the wear test. These samples had lost large amounts of material as shown in Figure 12 under an hour into the wear test.

Figure 12 Example of excessive wear volume

Figure 16 shows friction data from the sample containing 10wt% PP. It can be noted that the duration of this test is much shorter than that of the 25wt% PP sample. The COF for this specimen also fluctuates wildly. The wear scar produced by this test is comparable to that in Figure 12. The porous structure and resulting weakness is the

reason for high wear rate which also produces the inconsistent frictional behavior while causing the material to fail quickly. Figure 17 is a comparison of the two samples (25wt% PP and 10wt% PP). The contribution of nacreous pearl powder to wear resistance becomes very apparent in this comparison.

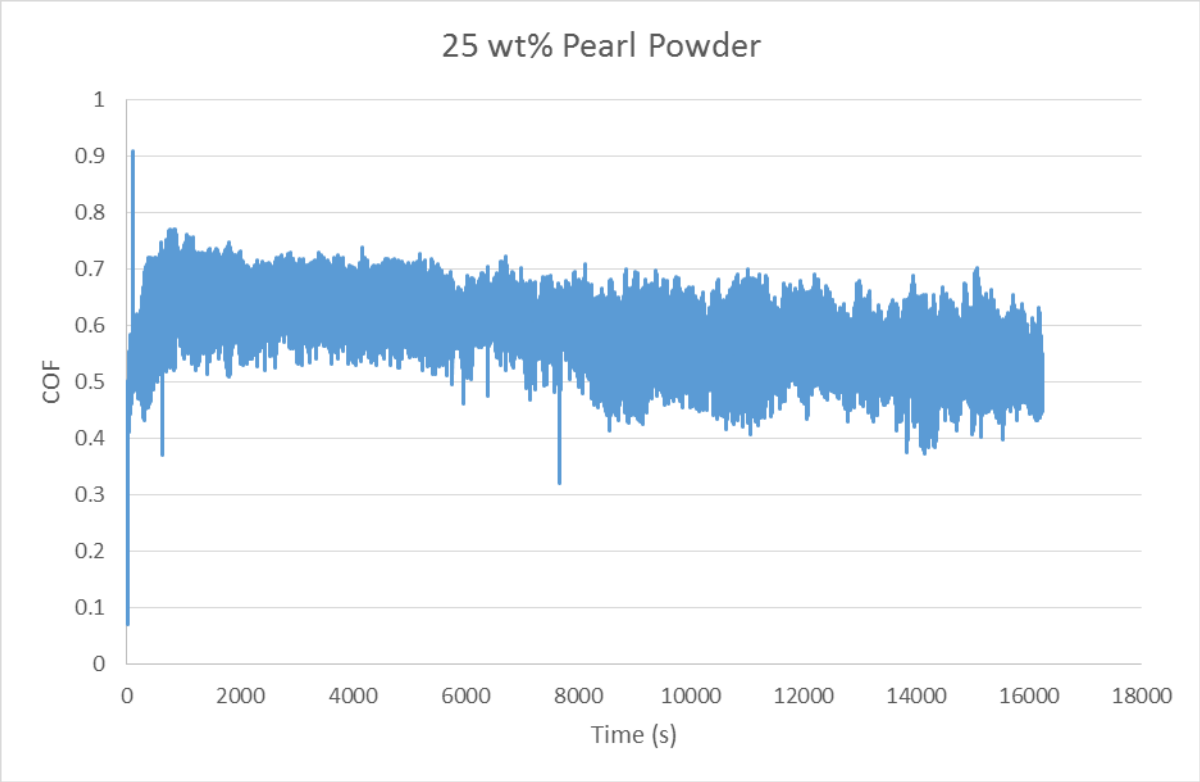

Figure 13 Friction data 25 wt% pearl powder

For the 25wt% PP sample, coefficient of friction levels out and remains consistent. Mean COF for this sample is 0.61 +/- 0.14. The consistent frictional behavior over such a long distance is indicative of a consistent microstructure and predictable interfacial behavior.

For the sample containing 25 wt% pearl powder there was a noted contribution of debris particles to COF. As noted earlier about particulate affecting wear and allowing for 3 body abrasion, this also affects the frictional behavior of the sample. Early in the wear tests (first hour) a gradual increase in COF was noticed. Midway through the test in Figure 14 debris was cleared to observe the contribution of debris. This is the cause of the sudden drop in COF about two hours into the test. The initial rise in COF due to the accumulation of wear debris is depicted in Figure 15. This indicates the interaction between the pin, debris, and samples.

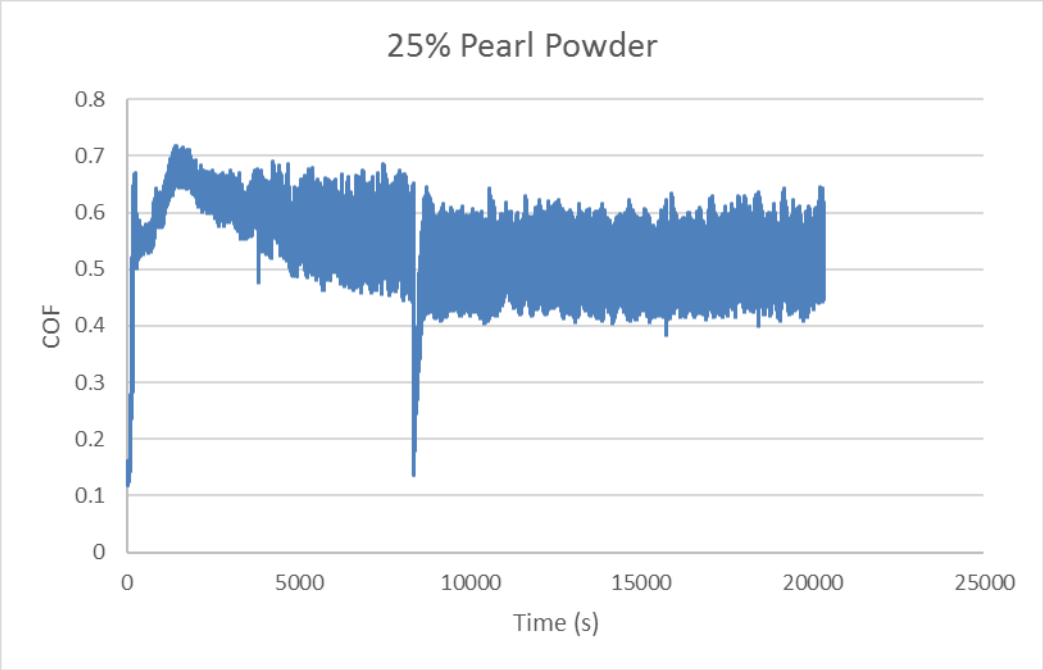

Figure 14 Friction data for showing debris effect

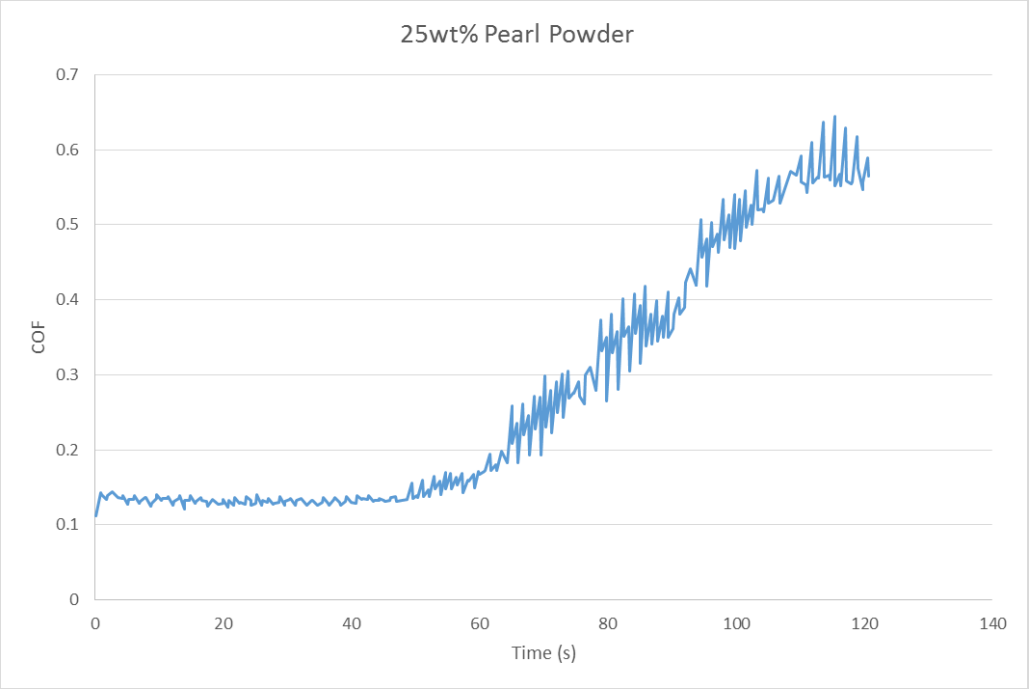

Figure 15 Pre-particulate behavior

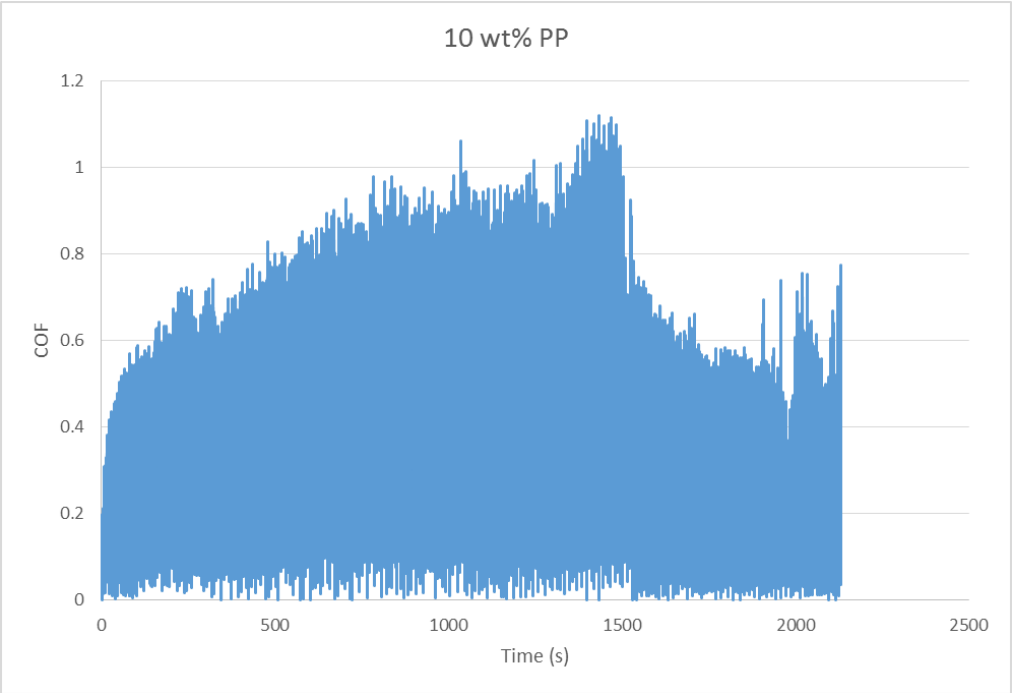

Figure 16 Friction data from 10wt% PP sample

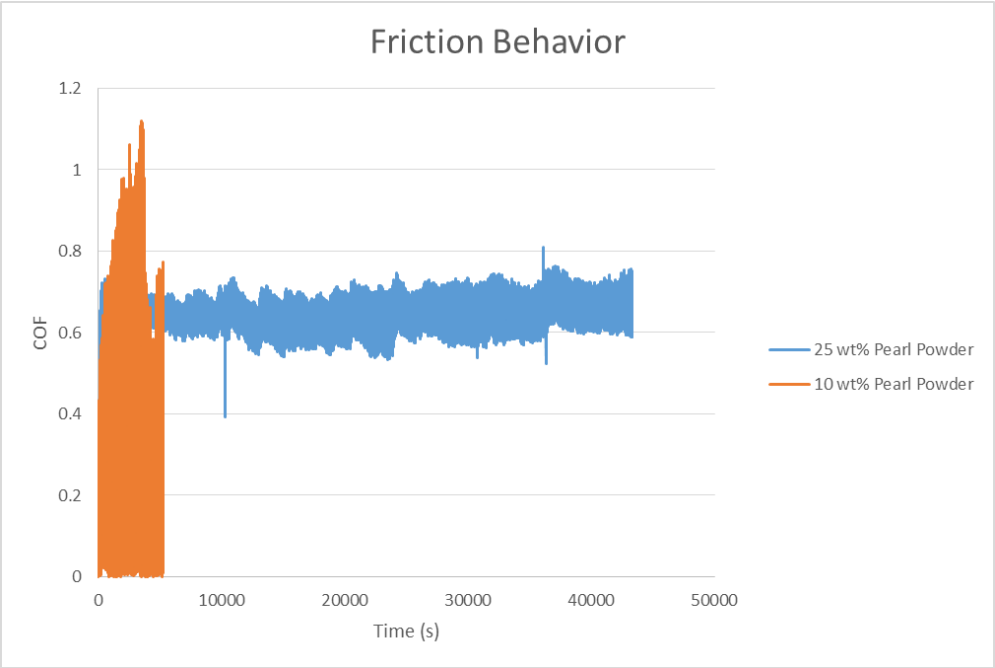

Figure 17 Comparison of 10 wt% to 25 wt%

The data presented above indicates a correlation between friction stabilization and wear resistance. Figure 17 shows the evidence of this relationship by comparing the friction data of 10wt%PP to that of 25wt%PP samples. While a specific value of COF against the steel pin is not that important, it is important to establish that friction behavior will stabilize and lead to high wear resistance.

4.2 Ranking Based on Corrosion Resistance

Because the human body is a corrosive environment, it is important for the proposed composite to be as noble as possible in ionic environments. Corrosion tests

were performed on the samples that showed better wear resistance based on the data in Table 5. The results of this are discussed below.

Figure 18 below shows the Current-Potential curve for the samples. In performing a Tafel estimation, the corrosion current and potential were calculated and reported below in Table 6 Corrosion data and decisions.

Corrosion current directly related to corrosion rate once corrosion begins. Corrosion potential, however is an indicator of a material's resistance to corrosion taking place.

It is evident from this data that the most corrosion resistant sample is that containing 33 wt% PP. It seems peculiar that adding PP to the 30 wt% and 25 wt% samples decreased the nobility of these samples. This trend is because the addition of the PP increases the porosity of the sample and thus the active surface area. The 33 wt% sample shows more corrosion resistance because there was more Ti in this sample which decreased the amount of active material at the surface. Another contributing factor is the increase in PP content. Though it seems to be a small difference, there is an increase in nobility from the 25 wt% sample to the 30 wt% sample. This indicates that the corrosion resistance property of the PP is beginning to overcome the resulting increase in active surface area.

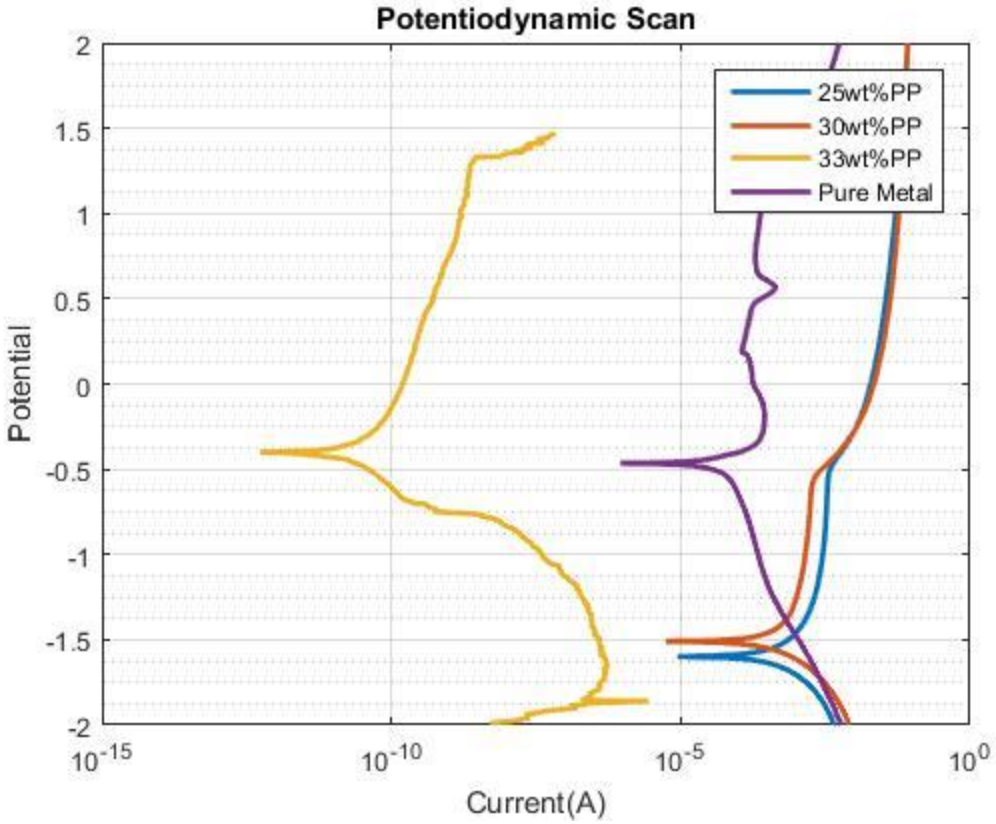

Figure 18 Corrosion behavior of samples

Sample	Corrosion Current (A)	Corrosion Potential (V)	Ranking
Pure Metal	9.20E-05	-5.35E-01	Control
33%PP	2.00E-11	-4.30E-01	Good corrosion resistance
30%PP	8.60E-04	-1.5	Improved from 25 wt%
25%PP	1.64E-03	-1.67	Less Resistance

Table 6 Corrosion data and decisions

4.3 Ranking Based on Porosity

Since wear and corrosion resistance are typically related to roughness and porosity of a material, it is important to see if there is a link between PP content and the porosity of a sample. Table 7 below shows measured porosity of the samples. It is evident that there is an optimum PP content for limiting porosity. While some porosity is necessary to ensure some surface roughness and high surface area for osteoconduction to occur, excessive porosity leads to decreasing wear and corrosion resistance. The exception being, of course, the 33 wt%PP samples. These exhibited better corrosion resistance due to the increased PP and Ti content.

Sample	Porosity (%)
10 wt%PP	8.231+/-0.928
25 wt%PP	0.412+/-0.003
30 wt%PP	1.248+/-0.009
33 wt%PP	2.790+/-0.050

Table 7 Porosity measurements

CHAPTER V

PERFORMANCE EVALUATION

This chapter discusses the performance of the selected samples against targeted conditions. These samples containing 33wt%, 30wt%, and 25wt% PP are characterized based on wear, friction, corrosion, bioactivity, and scratch resistance. The understanding of material performance establishes the validity of the concept of a PP enhanced composite for improving bone fixation.

5.1 Wear Behavior

While wear volume and wear rate are important for understanding how a material behaves it is also important to understand the type of wear occurring. The sample underwent different types of wear modes under different testing. When tested against the steel pin the sample exhibited two different wear modes while it did not wear against bone. The types of wear exhibited were two-body adhesive and abrasive wear. Two body wear simply means that only two surfaces were interacting. Over time, some three-body wear was exhibited against the steel pin because the debris from ongoing wear added to the abrasive wear going on in the test. Figure 19 shows how adhesive wear works. Adhesive wear occurs when a harder material (red) slides against a softer material (grey). The softer material will weld to the harder material and a small portion will be removed from the bulk of the original and stick to the harder material. Two-body abrasive wear as shown in Figure 20 occurs when two hard or brittle materials slide

against each other and asperities interact. The stronger material (red)breaks a piece off of the weaker material (blue).

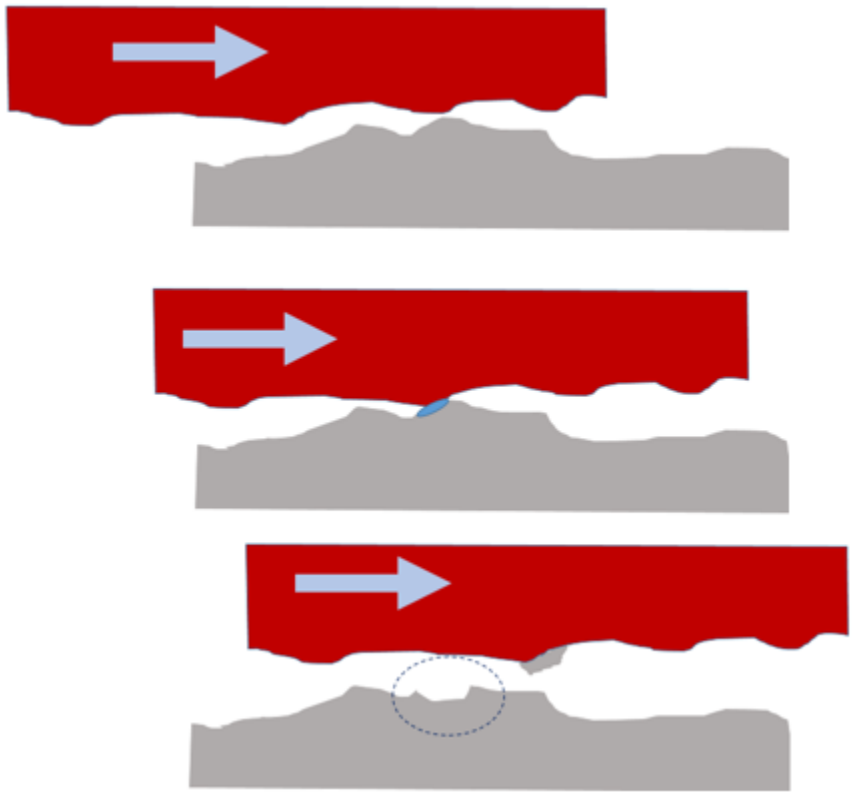

Figure 19 Adhesive wear

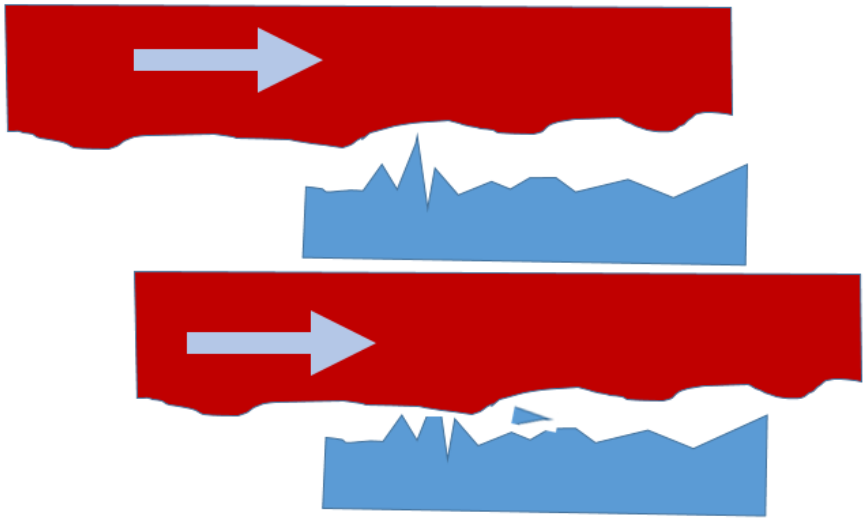

Figure 20 Abrasive wear

5.1.1 Steel Pin-on-Sample disk

Figure 21 is a picture of the wear track produced on the 25wt% pearl powder sample. The small wear track shows that this sample has some wear resistance. There is a reddish color from oxidized debris from the steel pin. Figure 22 shows the wear track immediately after the test prior to cleaning. The scar looks large due to the debris remaining on the scar and surrounding material.

Table 8 Wear volume due to steel pin of 25wt% PP sample below shows wear data for the 25 wt% PP sample. This is the sample which performed best under tribological conditions and produced minimal wear. The data for calculating the wear rate of this sample was obtained by examining microscope images like in Figure 24.

MEAN Depth (mm)	Mean Width (mm)	Mean Volume (mm^3)	Wear Rate (mm^3/s)
0.003136632	0.683936667	0.010726+/-.003	2.4746E-07

Table 8 Wear volume due to steel pin of 25wt% PP sample

Figure 21 Small wear track

Figure 22 Moderate wear volume

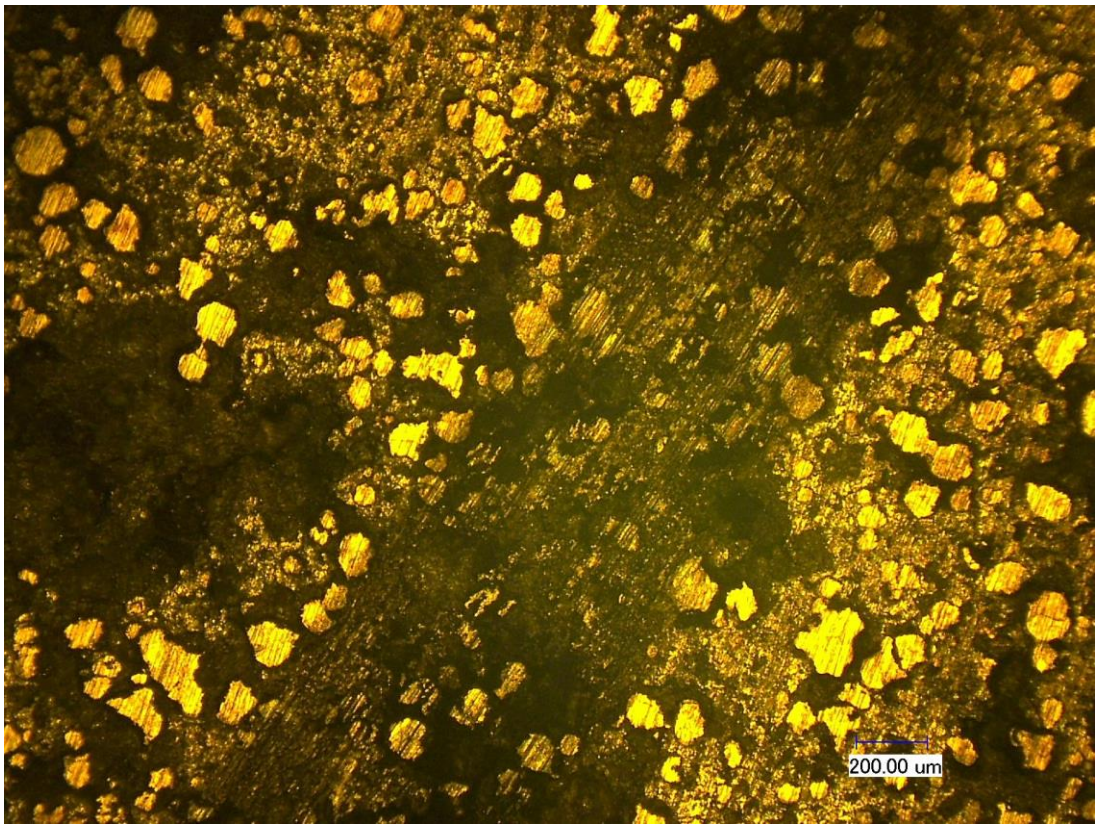

Figure 23 Wear scar due to steel ball

The figures below show characteristics of the wear mechanisms of the 25wt% PP sample. Figure 24 Wear on steel ball is a microscopic image of the steel ball after the wear test was performed. While the majority of the wear to the steel pin itself is abrasive wear, which is apparent based on the horizontal streaks and scars across the center of the bar. Oxidation of the ball can also be noted due to the reddish color throughout. This image makes it apparent that adhesive wear of the composite was occurring. Looking at Figure 23 Wear scar due to steel ball above it is hard to tell if any adhesive wear occurred because the sample is relatively porous compared to the steel ball. Therefore optical microscopy of the sample alone a less than ideal source for wear

analysis. Figure 25 SEM evidence of adhesive wearand Figure 24 show evidence of adhesive wear occurring. Particles appear to be stuck to the ball, and the SEM image indicates that there are areas where particles were pulled off of the surface of the sample material. This is not immediately apparent when examining Figure 26. Areas which don't show abrasive wear in this image, could merely be pores in the material where there would be no interaction. Figure 26 shows evidence of abrasive wear occurring during tests against the steel pin. Abrasive wear is evident by streaks on certain areas of the sample as indicated by areas circled in red in Figure 26.

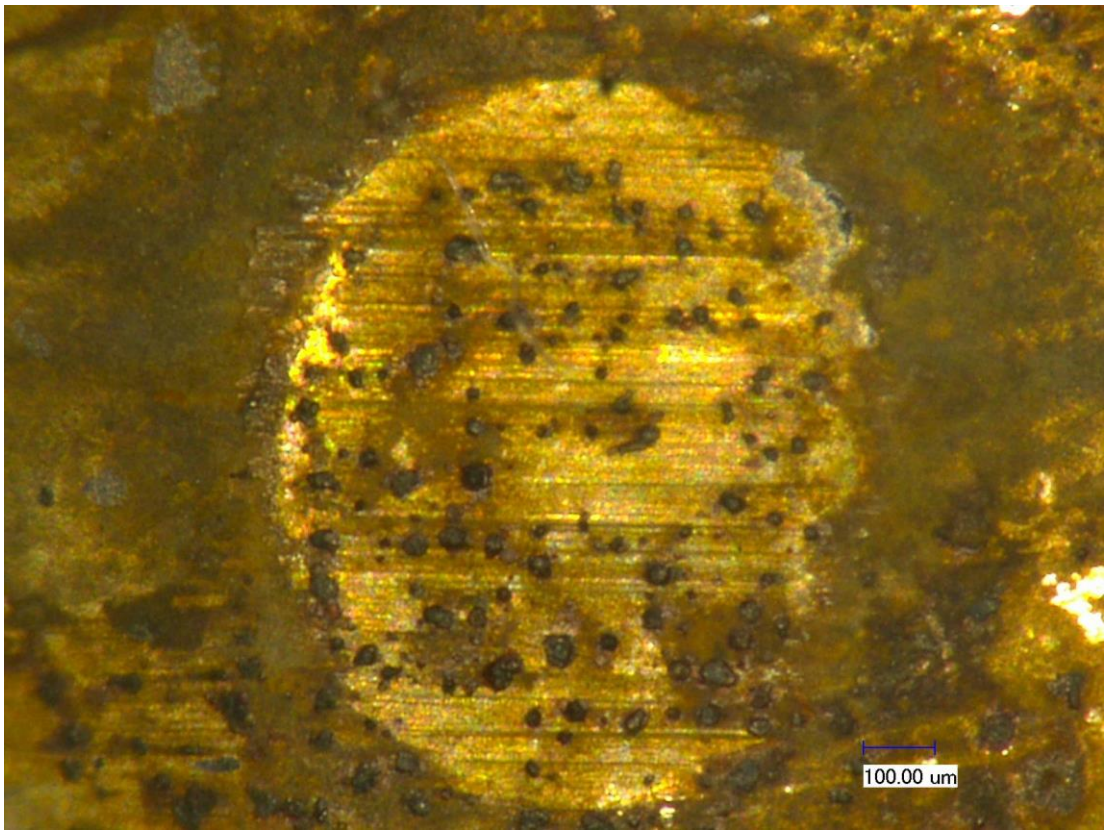

Figure 24 Wear on steel ball

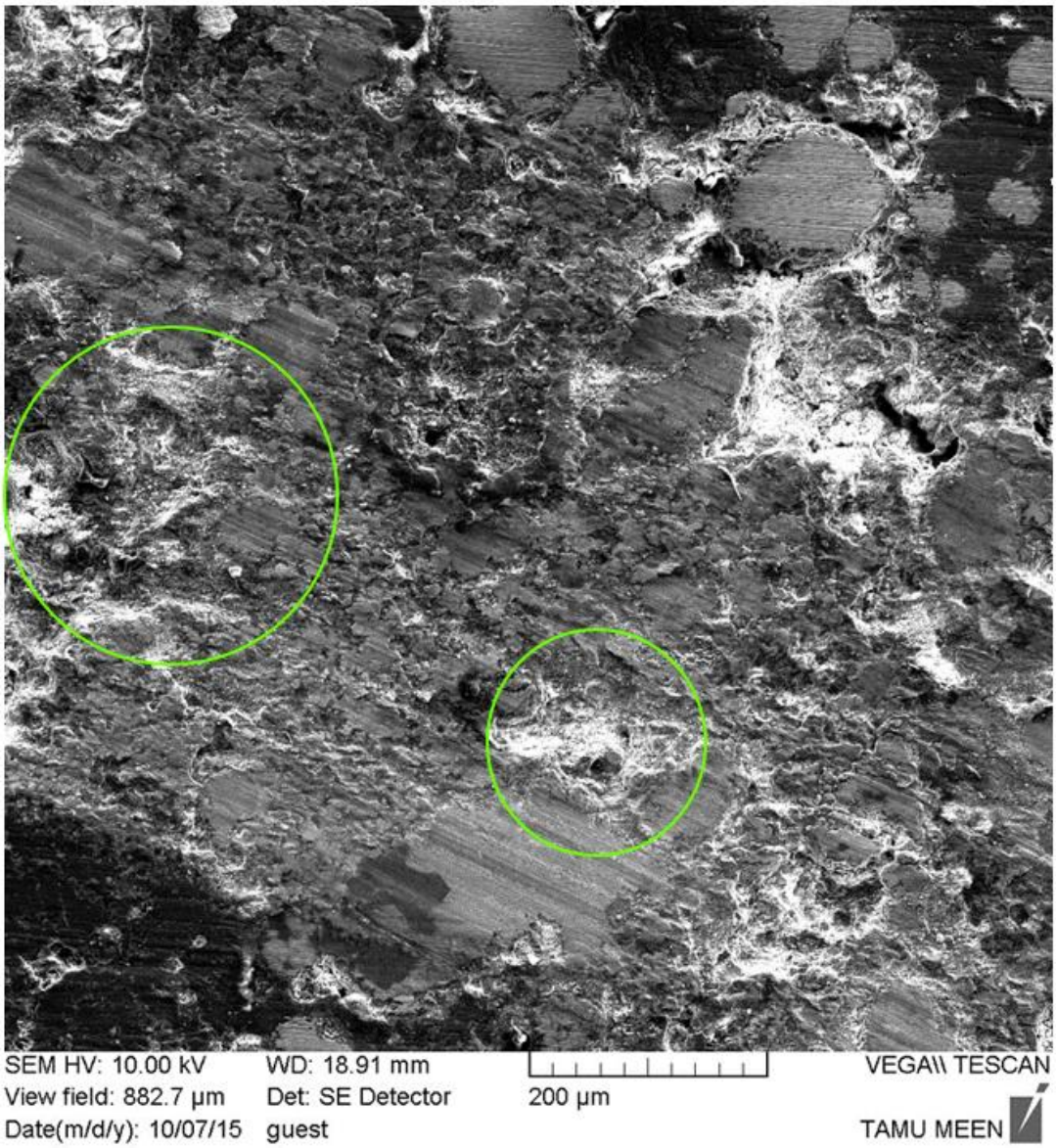

Figure 25 SEM evidence of adhesive wear

Figure 25 shows spots where adhesive wear has occurred, most adhesive wear of the sample appears to be near the interfaces between phases. While the softer aluminum gets pulled off, the harder titanium phase will not be so easily deformed plastically. It

does not want to stick to the steel pin and be removed so we see what seems to be pockets of adhesive wear right next to an area of abrasive wear.

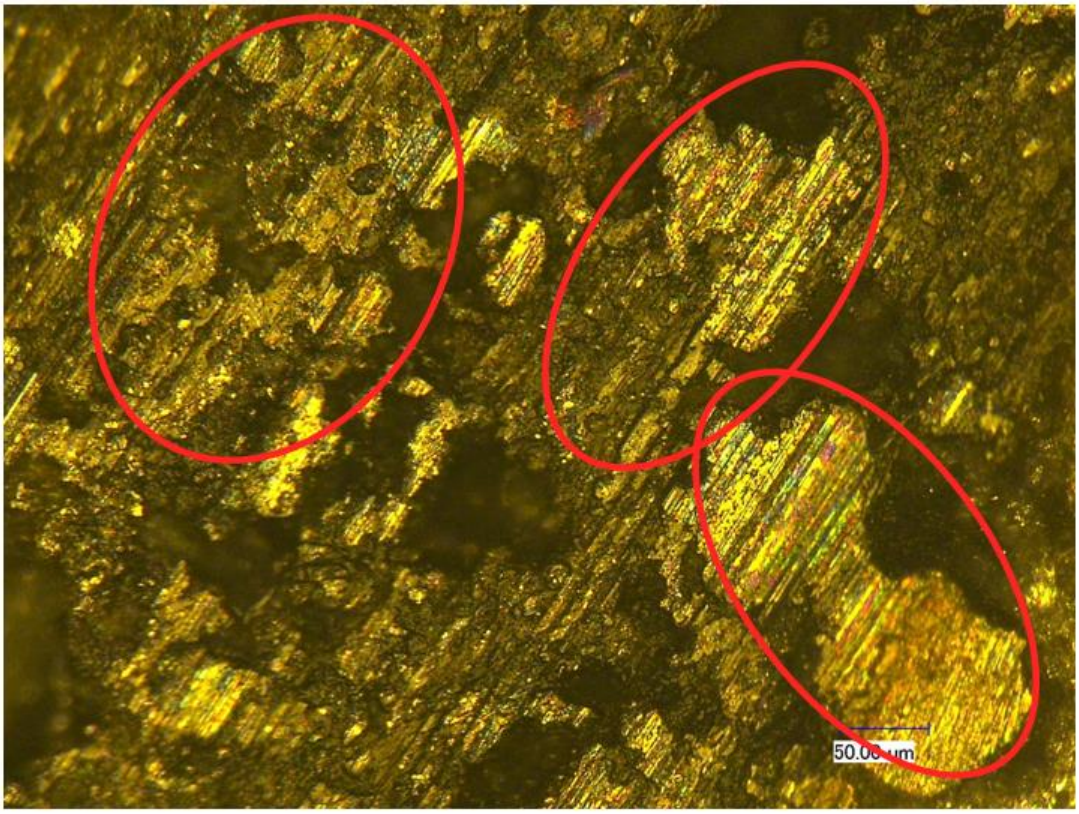

Figure 26 Evidence of abrasive wear

Being able to establish wear behavior is important to understand the characteristics of different phases on the surface and in the material. It also establishes the location of any weaknesses in the composite. The phases that exhibit abrasive wear tend to be the harder phases while softer, weaker phases can weld to the steel pin and be pulled off of the surface as they are held together as strongly.

5.1.2 Bone-on-Sample

This section shows the tribology of 25wt% unfiltered PP was studied against a bone from a pork chop.

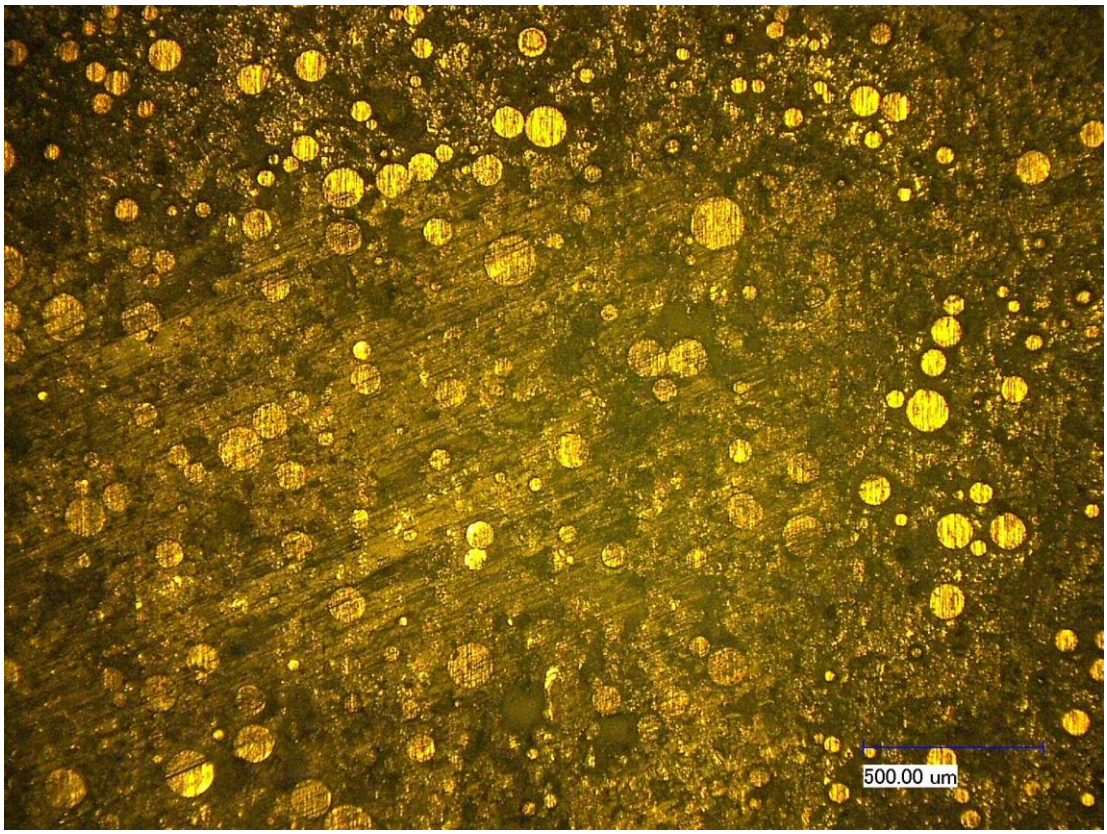

Figure 27 Wear scar of pork bone

After being tested against pork bone the samples did not wear out themselves, but the bone did wear against the sample since it is a much softer material. Figure 27 shows the wear scar produced from the pork bone wearing on the sample. Figure 28

makes it clear to see that the bone has left residue or film onto the sample. There is a slight discoloration in the area circled in red.

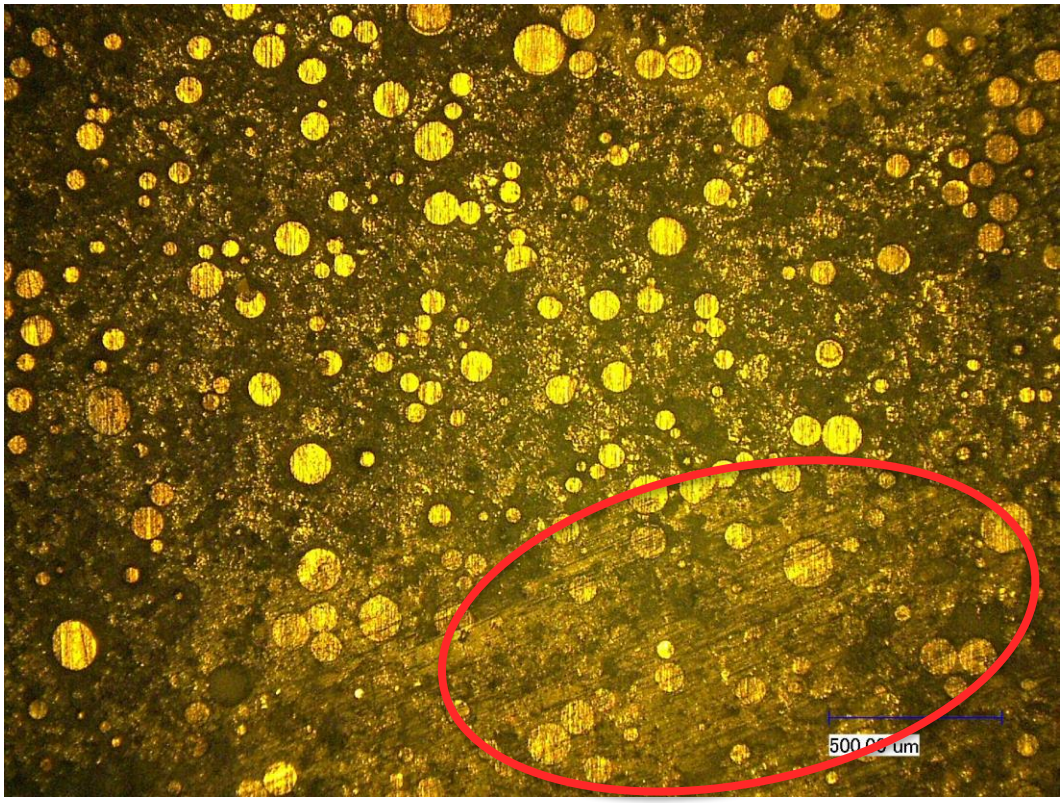

Figure 28 Discoloration evident from bone wear

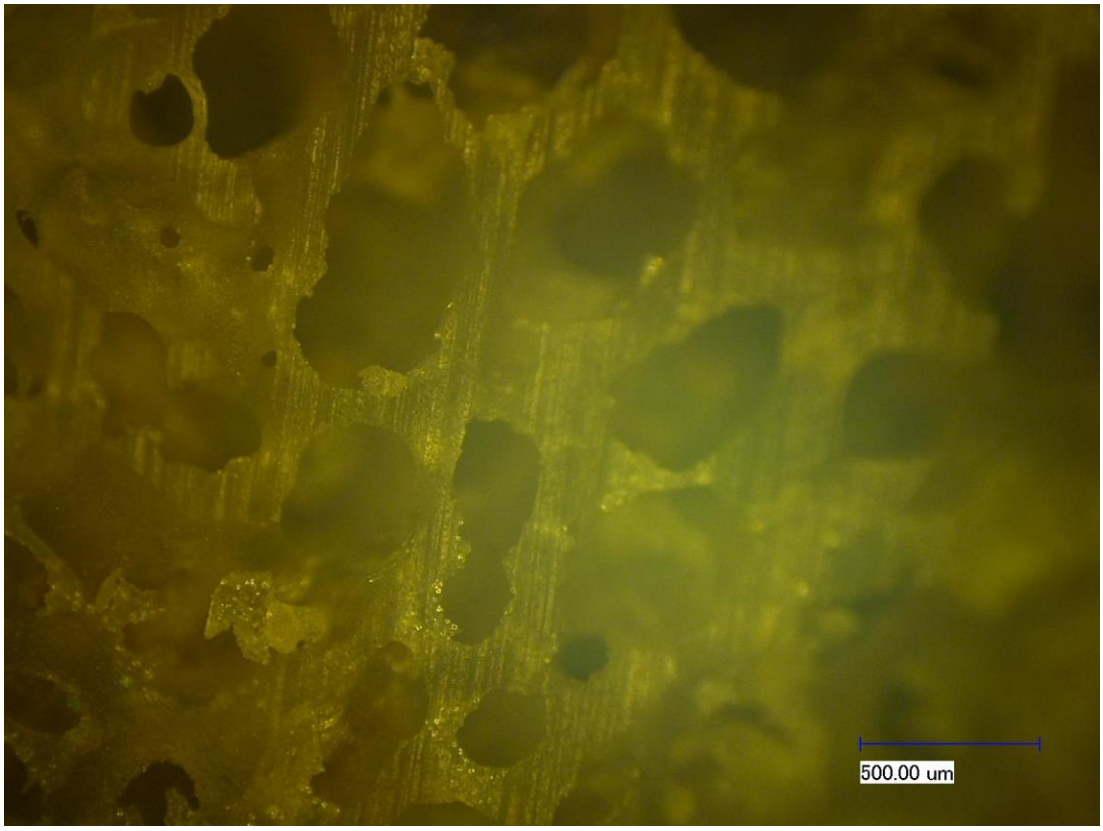

Figure 29 Image of bone wear

Figure 29 shows the scar that the sample left on the bone after the wear test. There is no evidence of adhesive wear, but abrasive wear is evident through the streaks apparent on the bone's surface. The large pores in the image are just part of the bone's structure. This is trabecular bone and is known for being soft and porous, giving bone a sort of sponge-like look.

Although bone wear is present, it is not excessive. In this study the amplitude of the reciprocation of the bone against the sample is larger than what would be expected in the use of this implant. This means it is more likely to wear the softer bone down.

Figure 30 shows that friction between the bone and implant stabilizes which is indicative or limited wear. This means the sample will not excessively wear out bone while it is in use.

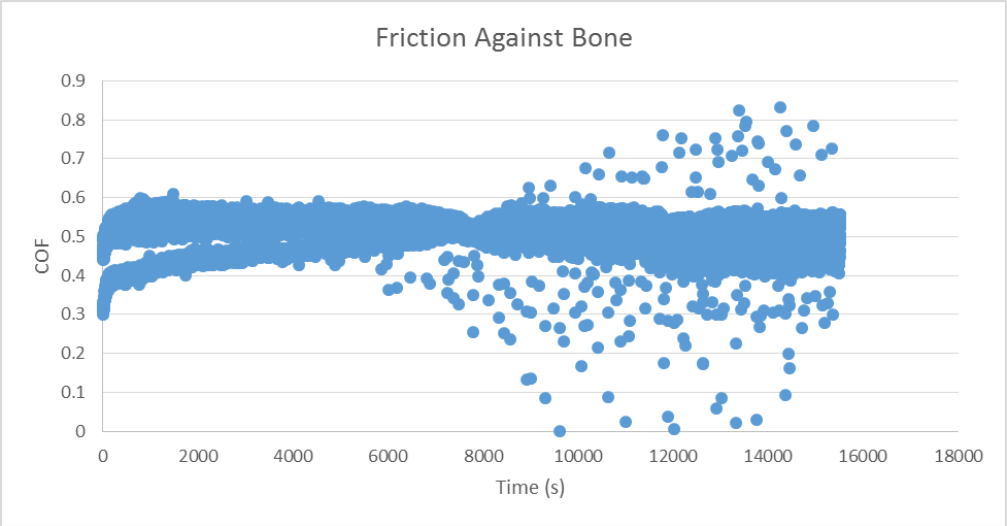

Figure 30 Friction stabilization against bone

.

5.2 Bioactivity Assessment

This section will discuss the viability of the samples as a bioactive material using simulated body fluid. After being immersed in SBF for 2 weeks, samples were removed and examined under SEM, optical microscope, and XRD.

5.2.1 Precipitation Evident from XRD Results

Below are XRD diffraction patterns for the 25wt% sample. Figure 31 shows XRD data on the sample prior to testing with SBF. Al and $CaCO_3$ peaks are evident, but Ti peaks are weak possibly because it is still amorphous. Figure 32 shows the data after

1 week in SBF. New peaks are apparent around 2Θ equals 10 and 25. These peaks are highlighted in the figure with red boxes. Though these peaks are not precisely that of hydroxyapatite, they are similar which indicate a similar structure. Any difference in 2-theta can be a result of the porosity of the samples. Figure 33 shows the peaks after longer exposure. An additional peak around 10 degrees is evident. It is stronger than in the 1 week immersion sample which is expected. XRD results indicate that precipitation did occur in SBF which means this composite shows promise as a bioactive material.

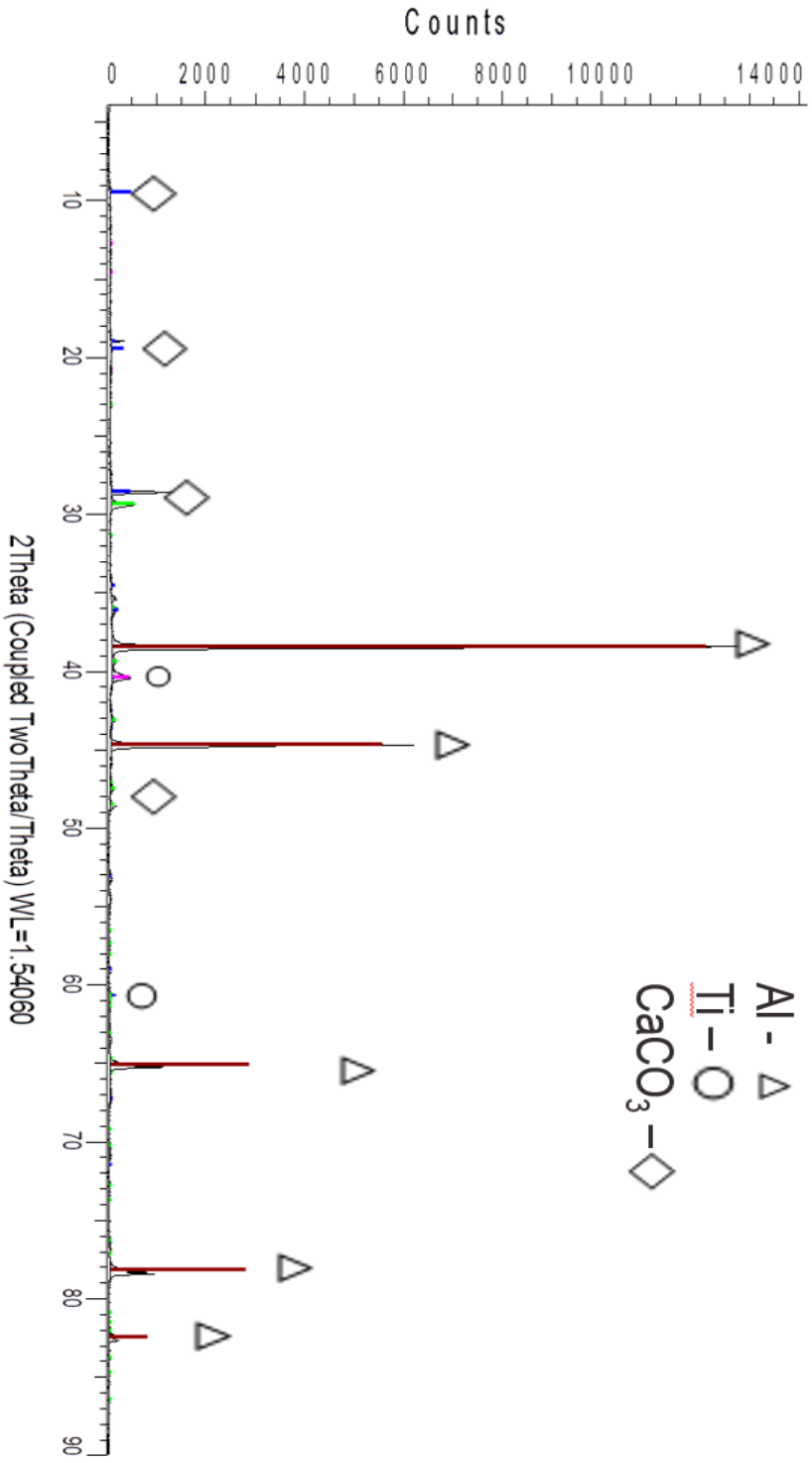

Figure 31 XRD pattern before SBF

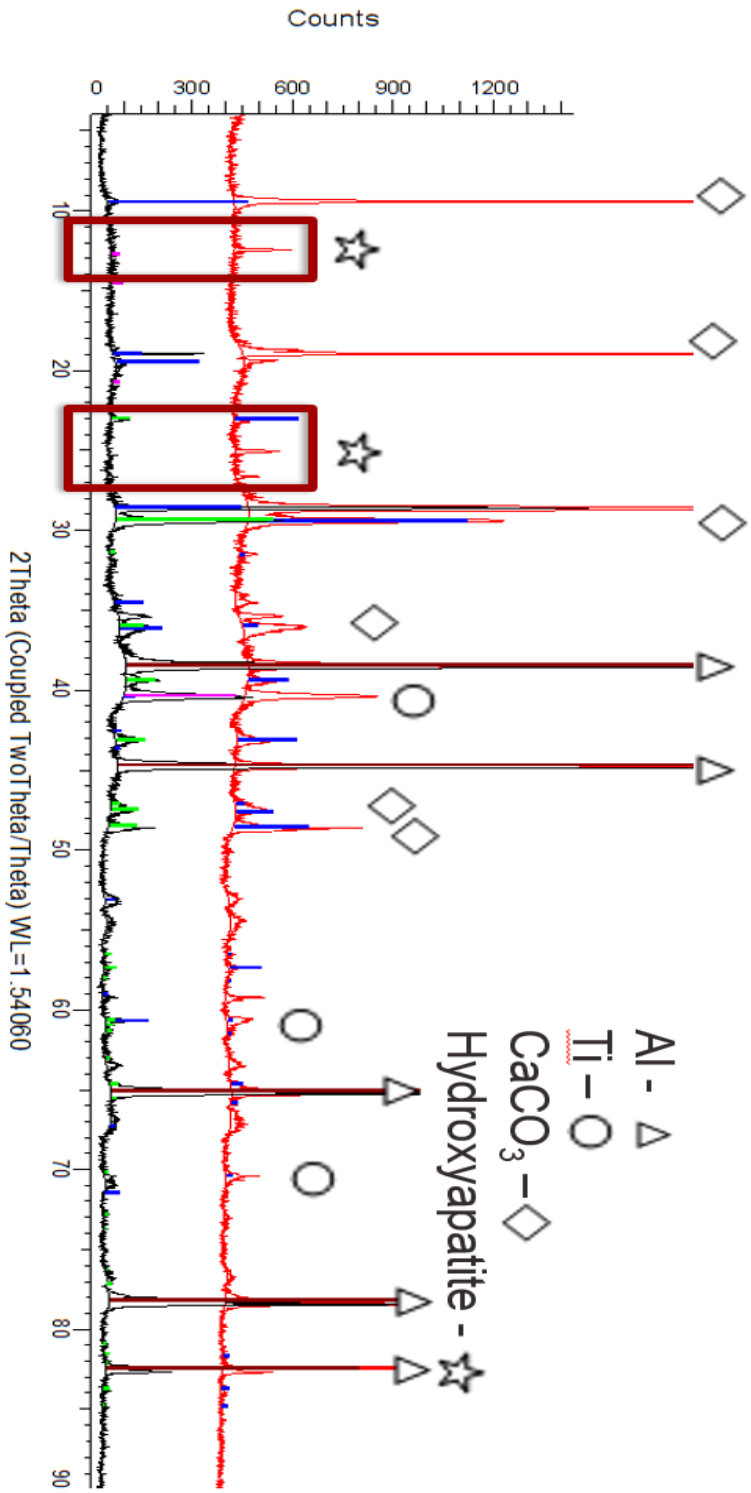

Figure 32 XRD pattern showing new peaks after SBF

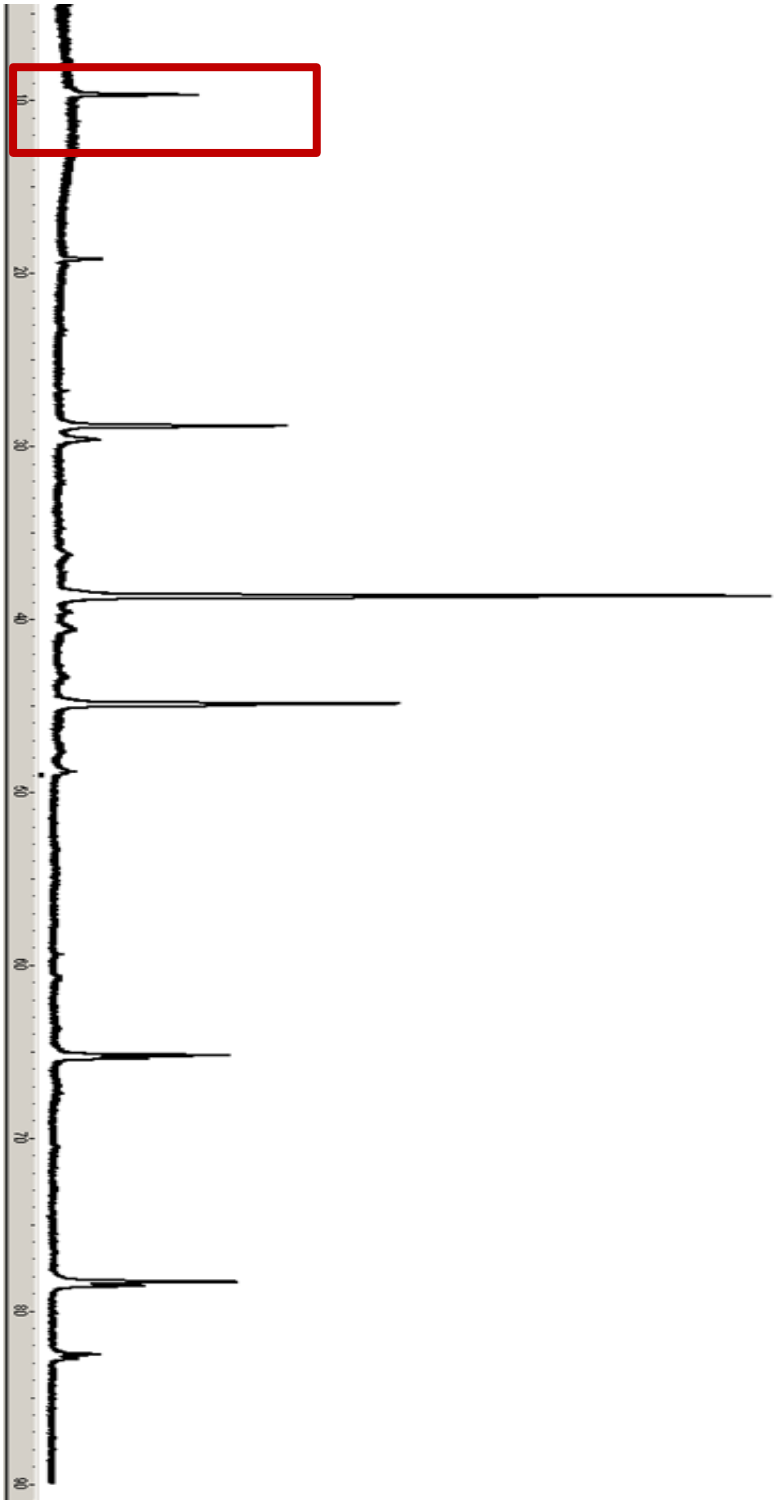

Figure 33 Pattern after 14 days

5.2.2 New Phase Identification using Microscopy

Both SEM and optical microscopy show evidence of precipitation after immersion in SBF. Figure 34 is an image of the sample surface prior to SBF immersion. This shows the different phases in the composite. Figure 35 is an image after the 14 day immersion. It appears that a film has formed on the surface as well as small precipitations. This provides further evidence that this composite has bioactive osteogenetic capabilities. Figure 36 and Figure 37 are close up images of the precipitation particles under optical microscope.

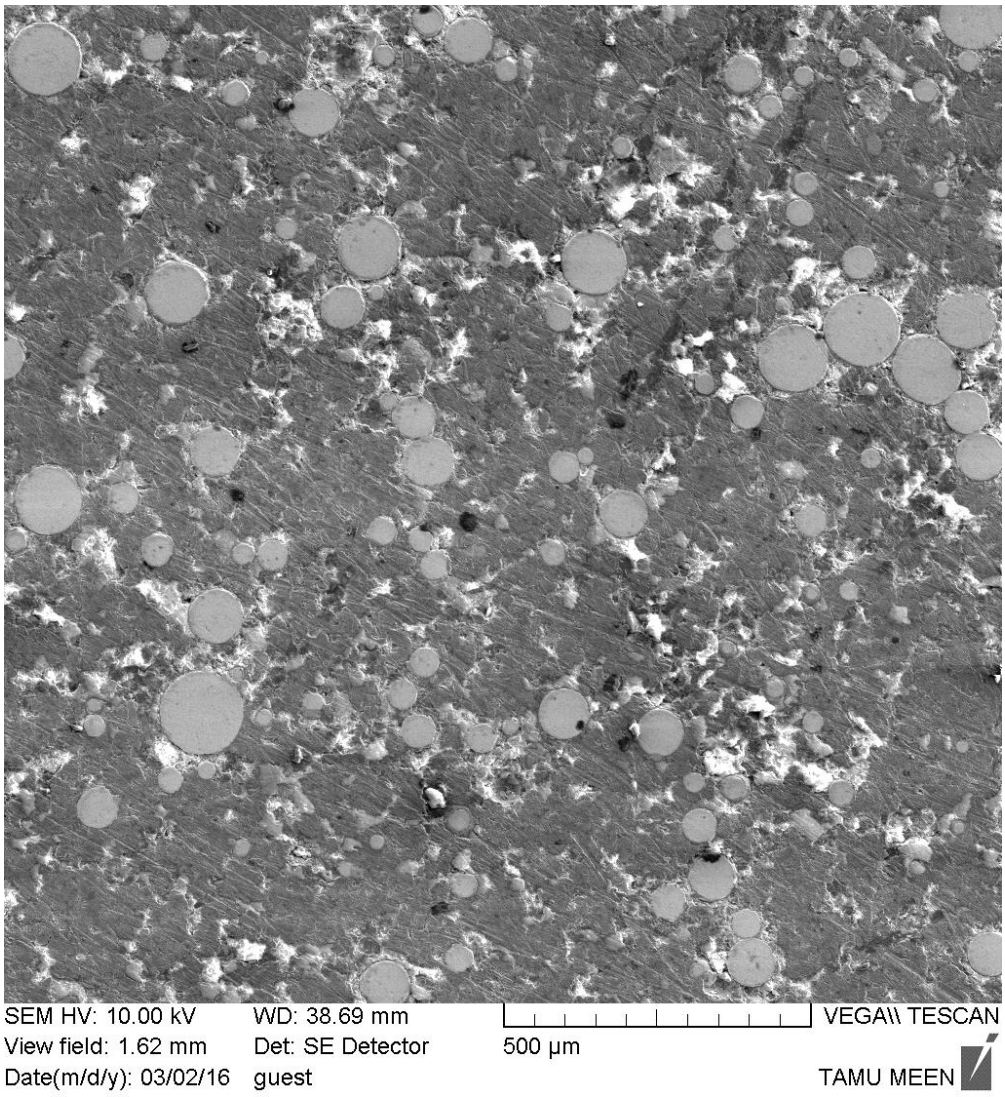

Figure 34 SEM image of sample prior to SBF

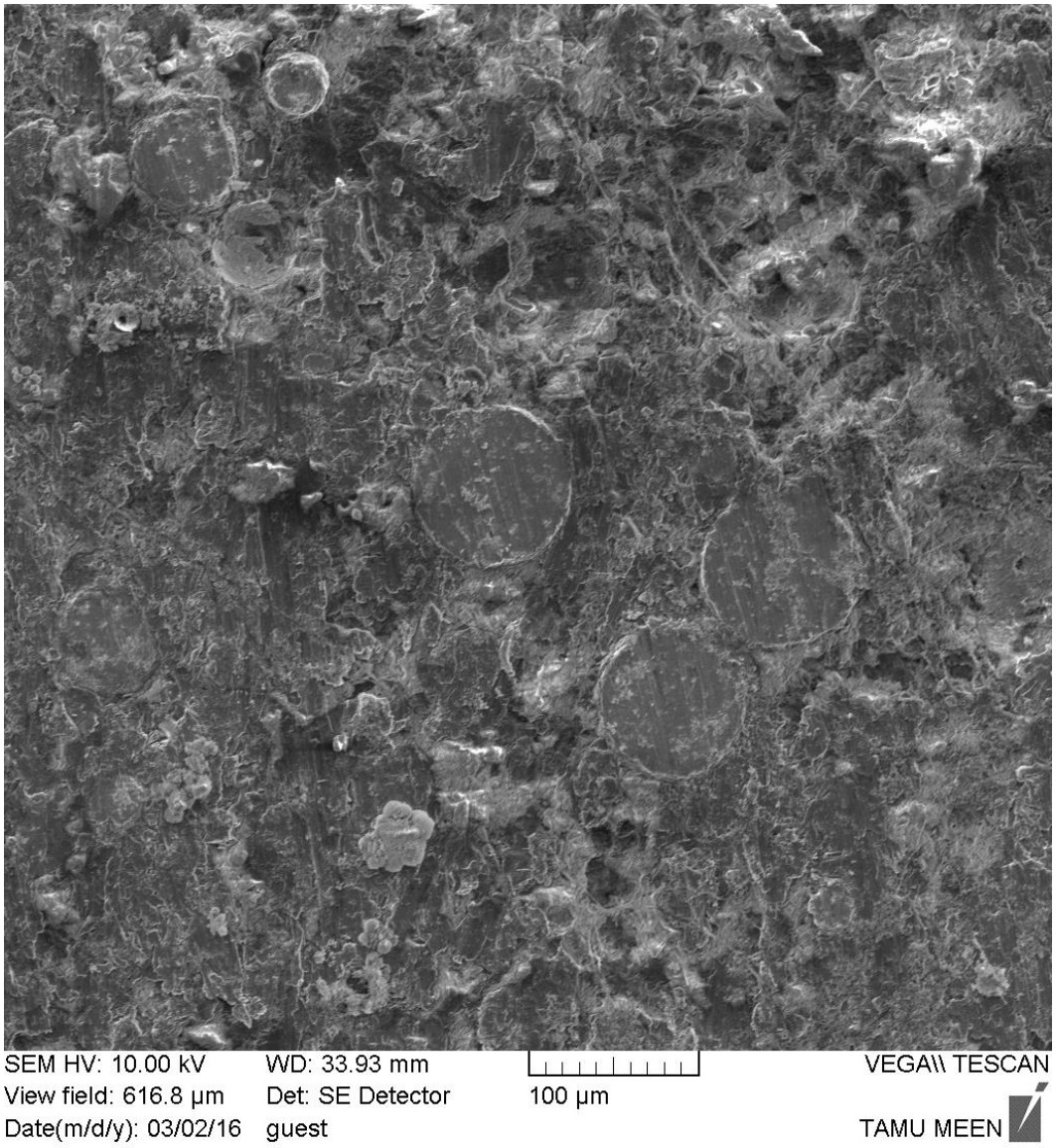

Figure 35 SEM image after SBF

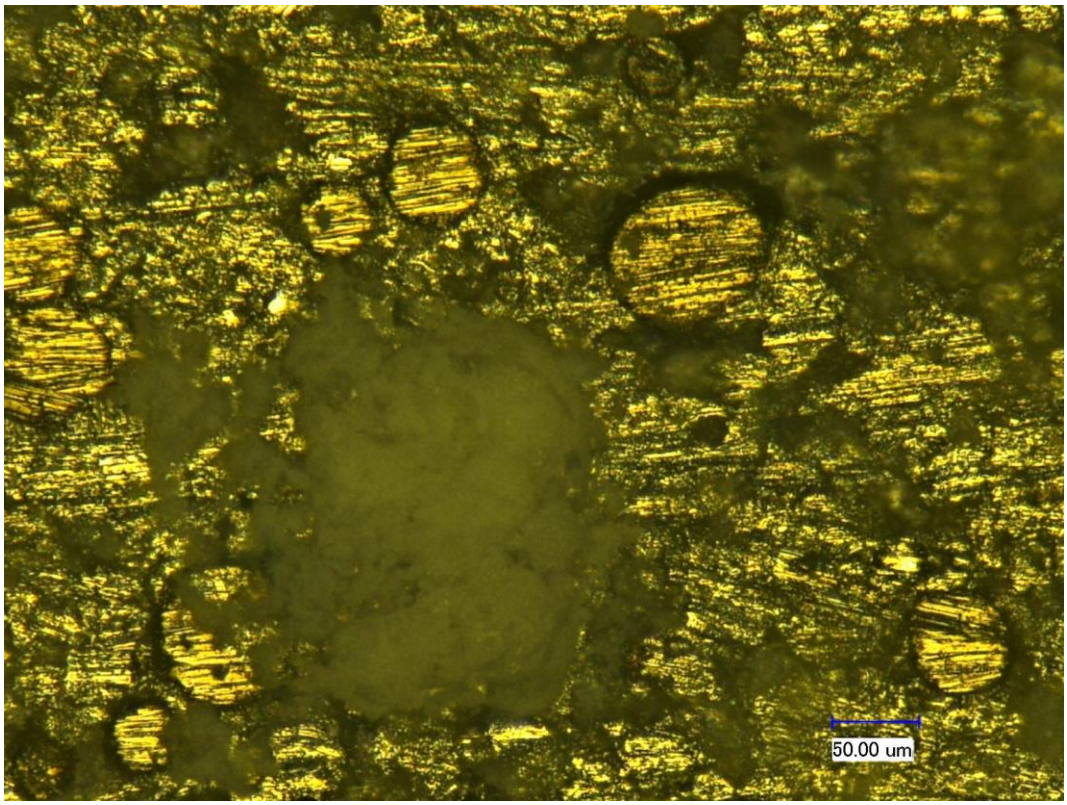

Figure 36 Precipitant under optical microscope

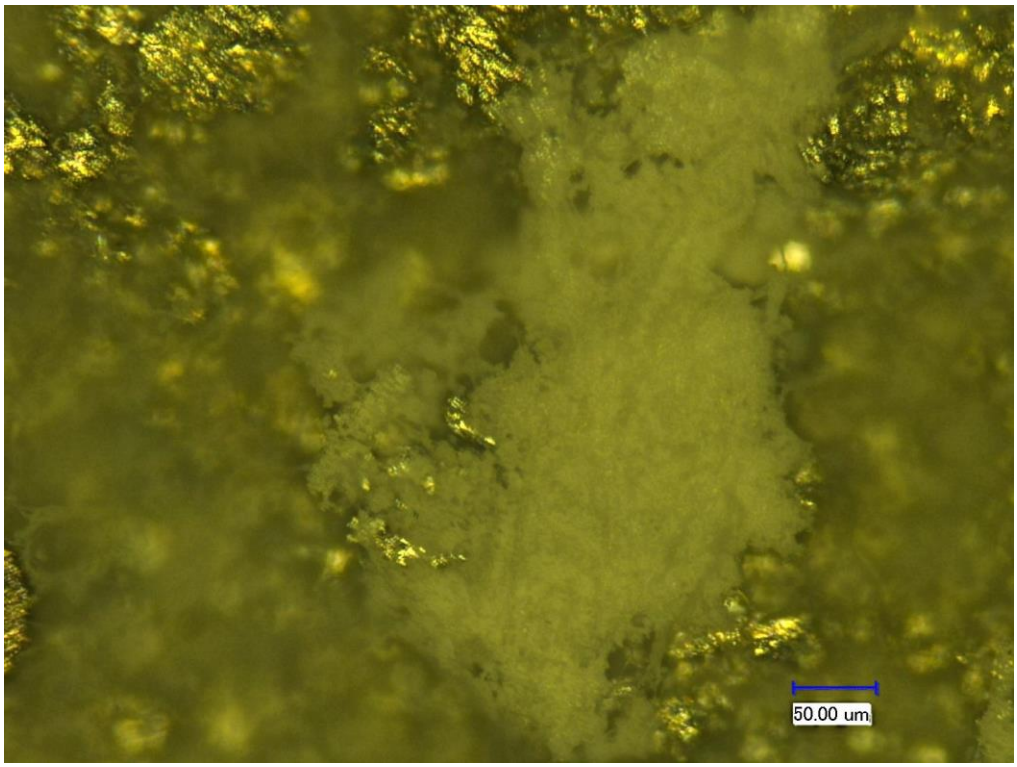

Figure 37 More precipitation particles

5.3 Scratch Resistance

Using Equation 1, fracture toughness was calculated. Table 9 shows the fracture toughness of the 33wt% and 25wt% samples. The measured parameter are listed in Table 9.

The drastic increase in toughness for the 25wt% sample demonstrates the impact that porosity has on the scratch resistance of the samples. The 25wt% sample shows fracture toughness on the order of that of trabecular bone.

Sample	Fracture Toughness
33wt%PP	0.569 Mpa$(m)^{1/2}$
25wt%PP	1.18 Mpa$(m)^{1/2}$

Table 9 Calculated fracture toughness

CHAPTER VI

CONCLUSIONS AND FUTURE RECOMMENDATIONS

6.1 Conclusions

This thesis reviewed current issues involving Total Disc Replacement. A novel composite was designed and fabricated. This material was studied as a potential improvement to Total Disc Replacement fixation.

Composite researched in this thesis utilizes nacre in two ways: it promotes osteoconductivity and protects the metal matrix in which it is embedded. Titanium is corrosion resistant and acts to strengthen the composite while the aluminum in the material acts as a binding matrix. Experiments showed that the sample containing 25wt% PP had the best tribological performance and fracture toughness but left something to be desired with respect to corrosion resistance. On the other hand, the weaker 33wt% PP sample showed better corrosion resistance with less than ideal tribological performance. All samples showed evidence of bioactivity, but no one sample could be established as the most bioactive or least. All formed precipitation layers and particles. Further investigation into this concept is required to find the ideal composition to maximize wear resistance, scratch resistance, corrosion resistance, and bioactivity. This research shows that nacre-enhanced composites show promise as a material to enhance the bone-implant interface of Total Disc Replacements.

6.2 Future Recommendations

Finding optimal material components and concentrations thereof are still required. Nacre is established for being a good substitute and can retain its properties when used as an enhancing material for a composite. This indicates that a limiting factor of this design is the matrix which is modified by nacre. Further tests for bioactivity and compatibility are still required for this material.

REFERENCES

1. Schiller, J., et al., *Summary Health Statistics for U.S. Adults: National Health Interview Survey, 2010.* Vital Health Stat, 2012. **10**(252).

2. Karajan, N., *Multiphasic Intervertebral Disc Mechanics: Theory and Application.* Archives of computational methods in engineering, 2012. **19**(2): p. 261-339.

3. Lazennec, J.Y., et al., *Clinical outcomes, radiologic kinematics, and effects on sagittal balance of the 6 df LP-ESP lumbar disc prosthesis.* Spine J, 2014. **14**(9): p. 1914-20.

4. Neumann, D.A., *Kinesiology of the musculoskeletal system: foundations for rehabilitation*. 2013: Elsevier Health Sciences.

5. Bogduk, N., *Clinical anatomy of the lumbar spine and sacrum*. 2005.
6. Markolf, K.L. and J.M. Morris, *The structural components of the intervertebral disc.* J Bone Joint Surg, 1974. **56**(4): p. 675-687.

7. Rothman, R.H. and F.A. Simeone, *The spine.* Journal of Pediatric Orthopaedics, 1992. **12**(4): p. 549.

8. Gloria, A., et al., *A multi-component fiber-reinforced PHEMA-based hydrogel/HAPEX device for customized intervertebral disc prosthesis.* J Biomater Appl, 2011. **25**(8): p. 795-810.

9. Knapik, G., *Use of a personalized hybrid biomechanical model to assess change in lumbar spine function with a TDR compared to an intact spine.* European spine journal, 2012. **21**(5): p. 641-652.

10. Serhan, H., et al., *Motion-preserving technologies for degenerative lumbar spine: The past, present, and future horizons.* SAS Journal, 2011. **5**(3): p. 75-89.

11. Gornet, M.F., et al., *Lumbar disc arthroplasty with Maverick disc versus stand-alone interbody fusion: a prospective, randomized, controlled, multicenter investigational device exemption trial.* Spine (Phila Pa 1976), 2011. **36**(25): p. E1600-11.

12. Kumar, M., *Correlation between sagittal plane changes and adjacent segment degeneration following lumbar spine fusion.* European spine journal, 2001. **10**(4): p. 314-319.

13. Kumar, M., *Long-term follow-up of functional outcomes and radiographic changes at adjacent levels following lumbar spine fusion for degenerative disc disease.* European spine journal, 2001. **10**(4): p. 309-313.

14. Cakir, B., et al., *Resect or not to resect: the role of posterior longitudinal ligament in lumbar total disc replacement.* European Spine Journal, 2012. **21**(5): p. 592-598.

15. Schulte, T., *Acquired spondylolysis after implantation of a lumbar ProDisc II prosthesis: Case report and review of the literature.* Spine (Philadelphia, Pa. 1976), 2007. **32**(22): p. E645-E648.

16. Veruva, S.Y., et al., *Which design and biomaterial factors affect clinical wear performance of total disc replacements? A systematic review.* Clinical Orthopaedics and Related Research®, 2014. **472**(12): p. 3759-3769.

17. Tomoyuki Takigawa, M., PhD,*† Alejandro A. Espinoza Orías, PhD,* Howard S. An, MD,*, M. Satoshi Gohgi, * Ranjith K. Udayakumar, MBBS,* Keizo Sugisaki, MD, PhD,*, and P. Raghu N. Natarajan, * Markus A. Wimmer, PhD,* and Nozomu Inoue, MD, PhD*, *Spinal Kinematics and Facet Load Transmission After Total Disc Replacement.* SPINE 2010. **35**(22): p. E1160-E1166.

18. Kettler, A., M. Bushelow, and H.J. Wilke, *Influence of the loading frequency on the wear rate of a polyethylene-on-metal lumbar intervertebral disc replacement.* Eur Spine J, 2012. **21 Suppl 5**: p. S709-16.

19. Shkolnikov, Y.P., et al., *Wear pattern observations from TDR retrievals using autoregistration of voxel data.* J Biomed Mater Res B Appl Biomater, 2010. **94**(2): p. 312-7.

20. Wen-Ming Chen, M., * ChunKun Park, MD, PhD,† KwonYong Lee, PhD,‡ and P. and SungJae Lee, *In Situ Contact Analysis of the Prosthesis Components of Prodisc-L in Lumbar Spine Following Total Disc Replacement.* SPINE 2009. **34**(20): p. E716–E723.

21. Huang, R.C., et al., *The implications of constraint in lumbar total disc replacement.* Journal of spinal disorders & techniques, 2003. **16**(4): p. 412-417.

22. Austen, S., et al., *Clinical, radiological, histological and retrieval findings of Activ-L and Mobidisc total disc replacements: a study of two patients.* Eur Spine J, 2012. **21**(Suppl 4): p. S513-S520.

23. Bao, Q.-B., et al., *Nubac disc arthroplasty: preclinical studies and preliminary safety and efficacy evaluations.* SAS Journal, 2007. **1**(1): p. 36-45.

24. Marchi, L., et al., *The importance of the anterior longitudinal ligament in lumbar disc arthroplasty: 36-Month follow-up experience in extreme lateral total disc replacement.* The International Journal of Spine Surgery, 2012. **6**(1): p. 18-23.

25. McNally, D., J. Naylor, and S. Johnson, *An in vitro biomechanical comparison of Cadisc™-L with natural lumbar discs in axial compression and sagittal flexion.* European Spine Journal, 2012. **21**(5): p. 612-617.

26. Pimenta, L., et al., *Clinical performance of an elastomeric lumbar disc replacement: Minimum 12 months follow-up.* SAS Journal, 2010. **4**(1): p. 16-25.

27. van den, B., *Design of next generation total disk replacements.* Journal of Biomechanics, 2012. **45**(1): p. 134-140.

28. Credo Reference (Firm), *Merriam-Webster's medical desk dictionary*. 2006, Thomson Delmar Learning,: Clifton Park, N.Y. p. 1 online resource.

29. Kang, J., *Chronic Failure of a Lumbar Total Disc Replacement with Osteolysis. Report of a Case with Nineteen-Year Follow-up.* JBJS The Journal of Bone & Joint Surgery, 2008. **90**(10): p. 2230.

30. Bisseling, P., et al., *Metal ion levels in patients with a lumbar metal-on-metal total disc replacement SHOULD WE BE CONCERNED?* Journal of Bone & Joint Surgery, British Volume, 2011. **93**(7): p. 949-954.

31. Black, J., *In vivo corrosion of a cobalt-base alloy and its biological consequences*, in *Biocompatibility of Co-Cr-Ni alloys*. 1988, Springer. p. 83-100.

32. Taksali, S., J.N. Grauer, and A.R. Vaccaro, *Material considerations for intervertebral disc replacement implants.* Spine J, 2004. **4**(6 Suppl): p. 231S-238S.

33. Agarwal, S., *Osteolysis - basic science incidence and diagnosis.* Current Orthopaedics, 2004. **18**: p. 220-231.

34. Hallab, N., *A review of the biologic effects of spine implant debris: Fact from fiction.* SAS journal, 2009. **3**(4): p. 143-160.

35. Per Aspenberg, P.H., *Periprosthetic bone resorption. Particles versus movement* J Bone Joint Surg Br 1996. **78**(4): p. 641-646.

36. Shin, Y., X. Huaping, and L. Hong, *A Novel Composite With Nacreous Reinforcement for Corrosion and Wear Reduction.* Journal of Tribology, 2015. **137**(2): p. 1-8.

37. Xiao, H., et al., *A new composite designed to resist wear.* Materials & Design, 2014. **63**: p. 749-756.

38. Pascaretti-Grizon, F., et al., *The interface between nacre and bone after implantation in the sheep: a nanotomographic and Raman study.* Journal of Raman Spectroscopy, 2014. **45**(7): p. 558-564.

39. Yang, Y.-L., et al., *Osteogenic activity of nanonized pearl powder/poly (lactide-co-glycolide) composite scaffolds for bone tissue engineering.* Bio-medical materials and engineering, 2013. **24**(1): p. 979-985.

40. Moutahir-Belqasmi, F., et al., *Effect of water soluble extract of nacre (Pinctada maxima) on alkaline phosphatase activity and Bcl-2 expression in primary cultured osteoblasts from neonatal rat calvaria.* Journal of Materials Science: Materials in Medicine, 2001. **12**(1): p. 1-6.

41. Almeida, M.J., et al., *Comparative effects of nacre water-soluble matrix and dexamethasone on the alkaline phosphatase activity of MRC-5 fibroblasts.* Journal of biomedical materials research, 2001. **57**(2): p. 306-312.

42. Mouriès, L.P., et al., *Bioactivity of nacre water-soluble organic matrix from the bivalve mollusk Pinctada maxima in three mammalian cell types: fibroblasts, bone marrow stromal cells and osteoblasts.* Comparative Biochemistry and Physiology Part B: Biochemistry and Molecular Biology, 2002. **132**(1): p. 217-229.

43. Rousseau, M., et al., *The water-soluble matrix fraction from the nacre of Pinctada maxima produces earlier mineralization of MC3T3-E1 mouse pre-osteoblasts.* Comparative Biochemistry and Physiology Part B: Biochemistry and Molecular Biology, 2003. **135**(1): p. 1-7.

44. Asvanund, P., P. Chunhabundit, and T. Suddhasthira, *Potential induction of bone regeneration by nacre: an in vitro study.* Implant dentistry, 2011. **20**(1): p. 32-39.

45. Milet, C., et al., *Conservation of signal molecules involved in biomineralisation control in calcifying matrices of bone and shell.* Comptes Rendus Palevol, 2004. **3**(6): p. 493-501.

46. Rousseau, M., et al., *Low molecular weight molecules of oyster nacre induce mineralization of the MC3T3-E1 cells.* Journal of Biomedical Materials Research Part A, 2008. **85**(2): p. 487-497.

47. Bhushan, B., *Modern Tribology Handbook, Two Volume Set*. 2000: Crc Press.

48. Kim, Y.-W., *Intermetallic alloys based on gamma titanium aluminide.* Jom, 1989. **41**(7): p. 24-30.

49. *Aluminum-Titanium Binary Phase Diagram.* ASM International Alloy Phase Diagram Database, 2014.

50. Wilke, H.J., et al., *New in vivo measurements of pressures in the intervertebral disc in daily life.* Spine, 1999. **24**(8): p. 755-762.

51. Kokubo, T. and H. Takadama, *How useful is SBF in predicting in vivo bone bioactivity?* Biomaterials, 2006. **27**(15): p. 2907-2915.

52. Akono, A., P. Reis, and F. Ulm, *Scratching as a fracture process: From butter to steel.* Physical review letters, 2011. **106**(20): p. 204302.

53. Chaiyabutr, Y., R. Giordano, and R. Pober, *The effect of different powder particle size on mechanical properties of sintered alumina, resin-and glass-infused alumina.* Journal of Biomedical Materials Research Part B: Applied Biomaterials, 2009. **88**(2): p. 502-508.